
ADV-0: Closed-Loop Min-Max Adversarial Training for Long-Tail Robustness in Autonomous Driving

Tong Nie^{1,2} Yihong Tang³ Junlin He¹ Yuewen Mei² Jie Sun² Lijun Sun³ Wei Ma¹ Jian Sun²

Abstract

Deploying autonomous driving systems requires robustness against long-tail scenarios that are rare but safety-critical. While adversarial training offers a promising solution, existing methods typically decouple scenario generation from policy optimization and rely on heuristic surrogates. This leads to objective misalignment and fails to capture the shifting failure modes of evolving policies. This paper presents ADV-0, a closed-loop min-max optimization framework that treats the interaction between driving policy (defender) and adversarial agent (attacker) as a zero-sum Markov game. By aligning the attacker’s utility directly with the defender’s objective, we reveal the optimal adversary distribution. To make this tractable, we cast dynamic adversary evolution as iterative preference learning, efficiently approximating this optimum and offering an algorithm-agnostic solution to the game. Theoretically, ADV-0 converges to a Nash Equilibrium and maximizes a certified lower bound on real-world performance. Experiments indicate that it effectively exposes diverse safety-critical failures and greatly enhances the generalizability of both learned policies and motion planners against unseen long-tail risks.

1. Introduction

Deploying autonomous driving (AD) systems in the open world faces a crucial bottleneck: the inability to anticipate and handle long-tail scenarios that are rare but safety-critical. While vast amounts of naturalistic driving data provide a basis for model development, they are dominated by normal logs, where high-risk events like aggressive cut-ins appear with negligible frequency (Liu & Feng, 2024; Xu et al., 2025b). The growing literature has introduced sampling and generative methods to accelerate the discovery of rare events (Feng et al., 2023; Ding et al., 2023). However, they are

often confined to stress testing or performance validation, failing to actively target long-tail risks. Effectively leveraging these synthetic data to improve the generalizability of AD policies in the long tail remains an open question.

Closed-loop adversarial training offers an avenue to address this challenge by exposing the training policy to synthetic risks. This paradigm can naturally be formulated as a min-max bi-level optimization problem via a zero-sum Markov game, involving an adversary that generates challenges and a defender that optimizes the policy (Pinto et al., 2017). Despite its theoretical elegance, direct application in AD and robotics has been hindered by nontrivial optimization issues. First, end-to-end solutions via gradient descent are often computationally intractable due to the non-differentiable nature of physical simulators and the difficulty of propagating gradients through long-horizon rollouts to provide learning signals. Second, the zero-sum interaction between two players is prone to instability and mode collapse (Zhang et al., 2020b), where the adversary converges to unrealistic attack patterns, limiting the scalability of this framework.

To bypass computational difficulties, existing methods typically decouple the min-max objective into separate sub-problems: generating scenarios via fixed priors or heuristics, then training the agent against this static distribution (Zhang et al., 2023; 2024; Stoler et al., 2025). However, this decoupled paradigm introduces notable limitations: (1) *Misaligned*. It creates a misalignment between the goals of the two players. While the defender optimizes a comprehensive reward that accounts for safety, efficiency, and comfort, the attacker solely targets collisions, relying on heuristic surrogates such as collision probability. First, this discrepancy renders the adversarial objective ill-defined, often resulting in an overly aggressive attacker that overwhelms the defender and destabilizes training (Zhang et al., 2020b). Second, the divergence in gradient directions prevents the attacker from identifying non-collision failures like off-road violations and providing meaningful learning signals. Thus, the defender can overfit to specific collision modes while remaining vulnerable to broader risks (Vinitzky et al., 2020), without acquiring generalized robustness. (2) *Nonstationary*. Decoupled methods with fixed attack modes fail to uncover the nonstationary vulnerabil-

¹The Hong Kong Polytechnic University, Hong Kong SAR, China ²Tongji University, Shanghai, China ³McGill University, Montreal, QC, Canada. Correspondence to: Wei Ma <wei.w.ma@polyu.edu.hk>, Jian Sun <sunjian@tongji.edu.cn>.

ity frontier—the shifting boundary of scenarios where the current policy remains prone to failure. As the defender evolves, its failure modes shift further into the long-tail distribution, becoming increasingly rare under the initial prior. Fixed adversaries with static priors are insufficient to track these shifting weaknesses, leading to fragile generalization in unseen risks. (3) *Uncertified*. Training against such static priors or heuristics acts as an empirical trial-and-error process, thus failing to provide theoretical safety guarantees. This lack of certified performance bounds contrasts sharply with the rigorous safety demands of real-world deployment, where agents must generalize to an unbounded variety of unknown long-tail scenarios (Brunke et al., 2022).

This work revisits the min-max formulation and introduces ADV-0, a closed-loop policy optimization framework that enables end-to-end training for generalizable adversarial learning. ADV-0 solves the Markov game by directly aligning the adversarial utility with the training objective of the defender. To address the tractability and stability issues, we propose an online iterative preference learning algorithm, casting adversarial evolution as preference optimization. This allows the attacker to continuously track the shifting vulnerability frontier of the improving defender. By coupling the evolution, ADV-0 tailors the distribution towards the long tail of the current players, forcing the defender to learn generalized robustness rather than overfitting to heuristics. Importantly, ADV-0 is algorithm-agnostic, applicable to both RL agents and motion planning models, providing a theoretically grounded pathway from adversarial generation to policy improvement. Our contributions are threefold.

- ADV-0 is the first closed-loop training framework for long-tail problems of AD that couples adversarial generation and policy optimization in an end-to-end way.
- We propose a preference-based solution to the zero-sum game, a stable and efficient realization supporting on-policy interaction and algorithm-agnostic evolution.
- Theoretically, ADV-0 converges to a Nash Equilibrium and maximizes a certified lower bound on real-world performances. Empirically, ADV-0 not only exposing diverse safety-critical events but also enhances the generalizability of policies against unseen long-tail risks.

2. Preliminary and Problem Formulation

Task description. We model the safe AD task as a Markov Decision Process (MDP), defined by $(\mathcal{S}, \mathcal{A}, \mathcal{P}, \mathcal{R}, \gamma, T)$. Here, \mathcal{S} and \mathcal{A} denote the state and action spaces. The state $s_t \in \mathcal{S}$ includes raw sensor inputs, high-level commands, and kinematic status. The action $a_t \in \mathcal{A}$ represents continuous low-level control signals (e.g., steering, acceleration). The environment dynamics $\mathcal{P} : \mathcal{S} \times \mathcal{A} \rightarrow \Delta(\mathcal{S})$ describe the transition probabilities of the traffic scene. We initialize scenarios using real-world driving logs, where the ego vehicle is controlled by a policy π_θ parameterized by θ .

Background traffic participants are initially governed by naturalistic behavior priors, such as log-replay or traffic models like the Intelligent Driver Model (IDM). The reward function $\mathcal{R}(s, a)$ is designed to balance task progress with safety: it encourages route completion and velocity tracking, while imposes heavy penalties for safety violations, such as collisions or off-road events. The goal of the ego agent is to learn an optimal policy π_θ^* that maximizes the expected cumulative return $J(\pi_\theta) = \mathbb{E}_{\tau \sim \pi_\theta, \mathcal{P}}[\sum_{t=0}^T \gamma^t \mathcal{R}(s_t, a_t)]$ within T . Unlike imitation learning which assumes a fixed data distribution, we focus on online RL to enable the agent to recover from adversarial perturbations in closed-loop interactions.

Min-max formulation. Relying solely on naturalistic scenarios often fails to expose the ego agent to low-probability but high-risk events residing in the long tail of the distribution. To ensure the robustness of the policy against long-tail risks, adversarial training frames the problem as a robust optimization task via a **two-player zero-sum game** between the ego agent and an adversary. Here, the behaviors of background agents are governed by a parameterized adversarial policy $\psi \in \Psi$ that alters the transition dynamics from the naturalistic \mathcal{P} to an adversarial \mathcal{P}_ψ . The robust policy optimization is thus cast as a min-max objective:

$$\max_{\theta} \min_{\psi \in \Psi} \left[J(\pi_\theta, \mathcal{P}_\psi) = \mathbb{E}_{\tau \sim (\pi_\theta, \mathcal{P}_\psi)} \left[\sum_{t=0}^T \gamma^t \mathcal{R}(s_t, a_t) \right] \right], \quad (1)$$

where Ψ represents the feasible set of adversarial configurations that remain physically plausible. The outer loop maximizes the ego’s performance, while the inner loop seeks an adversary that minimizes the current ego’s reward.

Directly optimizing the bi-level objective via gradient descent is often computationally intractable due to the non-differentiable nature of physical simulators and the difficulty of propagating gradients through long-horizon rollouts. Existing methods often decouple Eq. 1 into separate problems: (1) *Adversarial generation*: generating a static set of hard scenarios via surrogate objectives J_{adv} (e.g., collision probability); (2) *Policy optimization*: then optimizing π_θ against this fixed distribution. However, this decoupled paradigm introduces objective misalignment and fails to capture the non-stationary vulnerability frontier of the evolving policy.

3. The ADV-0 Framework

We introduce ADV-0, a closed-loop adversarial training framework to solve the min-max optimization problem in Eq. 1. Our approach treats the interaction between the driving agent (*defender*) and the traffic environment (*attacker*) as a dynamic *zero-sum game*: the defender minimizes the expected risk, while the attacker continuously explores the long-tail distribution to identify and exploit the ego’s evolving weaknesses. Due to the nonstationarity of the driving environment and the rarity of critical events, relying on

static datasets or heuristic adversarial priors is insufficient. Instead, we seek a Nash Equilibrium where the ego policy π_θ remains robust to the worst-case distributions generated by a continuously evolving adversary policy ψ . At this equilibrium, π_θ is theoretically guaranteed to perform well under any other distribution within the trust region. This section details this end-to-end bi-level optimization scheme.

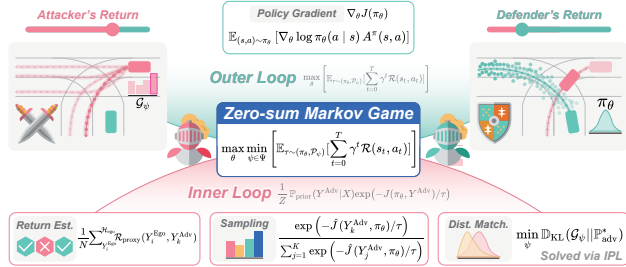


Figure 1. Illustration of the ADV-0 framework. It alternates between an *Inner Loop* where the adversary ψ evolves via IPL to track the failure frontier, and an *Outer Loop* where the ego π_θ optimizes policy gradients against the induced adversarial distribution.

3.1. End-to-End Framework for Min-Max Optimization

To enable tractability and stationarity, we propose an iterative end-to-end training pipeline inspired by Robust Adversarial Reinforcement Learning (RARL, Pinto et al. (2017)). The core of ADV-0 lies in efficiently propagating gradients from the ego’s objective J to the adversary ψ . The training alternates between two phases: (1) an *inner loop* that updates ψ to track the theoretical optimal attack distribution; and (2) an *outer loop* that optimizes the policy π_θ against the current induced distribution (Figure 1).

Inner loop. Formally, let X denote the context (e.g., map topology and initial traffic state) and Y^{Adv} denote the future adversarial trajectories. We define the critical event \mathcal{E} as the set of scenarios where the ego’s performance drops below a safety threshold ϵ : $\mathcal{E} := \{Y^{\text{Adv}} \mid J(\pi_\theta, Y^{\text{Adv}}) \leq \epsilon\}$. Then the attacker’s goal is to find an optimal adversarial distribution \mathbb{P}_{adv} that maximizes the likelihood of this critical event while constrained within the trust region of the naturalistic prior $\mathbb{P}_{\text{prior}}$. This is equivalent to a constrained optimization:

$$\begin{aligned} \max_{\mathbb{P}_{\text{adv}}} \mathbb{E}_{X \sim \mathcal{D}} \left[\mathbb{E}_{Y^{\text{Adv}} \sim \mathbb{P}_{\text{adv}}(\cdot|X)} [\log \mathbb{P}(\mathcal{E})] \right], \\ \text{s.t. } \mathbb{D}_{\text{KL}}(\mathbb{P}_{\text{adv}} \parallel \mathbb{P}_{\text{prior}}) \leq \delta. \end{aligned} \quad (2)$$

Directly solving Eq. 2 involves optimizing a hard indicator function $\mathbb{I}(Y^{\text{Adv}} \in \mathcal{E})$, suffering from vanishing gradients and event sparsity. To enable end-to-end gradient optimization, we relax the hard constraint into a soft energy function. We view the negative return $-J(\pi_\theta, Y^{\text{Adv}})$ as the unnormalized log-likelihood of the critical event. The objective is thus relaxed to maximizing the expected adversarial utility $\mathbb{P}(\mathcal{E}|Y^{\text{Adv}}) \approx \mathbb{E}_{Y^{\text{Adv}} \sim \mathbb{P}_{\text{adv}}} [-J(\pi_\theta, Y^{\text{Adv}})]$ within the trust region. By applying Lagrange multipliers, the optima $\mathbb{P}_{\text{adv}}^*$ can be derived in closed form as the Gibbs distribution:

$$\underbrace{\mathbb{P}_{\text{adv}}^*(Y^{\text{Adv}}|X)}_{\text{Posterior}} = \frac{1}{Z} \underbrace{\mathbb{P}_{\text{prior}}(Y^{\text{Adv}}|X)}_{\text{Traffic prior}} \underbrace{\exp(-J(\pi_\theta, Y^{\text{Adv}})/\tau)}_{\text{Generalized adversarial utility}}, \quad (3)$$

where Z is the partition function and τ is the temperature. Eq. 3 reveals that the theoretically optimal adversary reweights the traffic prior based on the generalized adversarial utility (GAU). Traffic prior ensures plausibility, and GAU is the likelihood that Y^{Adv} causes the current policy π_θ to fail. However, directly sampling from $\mathbb{P}_{\text{adv}}^*(\cdot|X)$ is intractable due to the unknown partition function. ADV-0 solves for this via a two-step approximation: (1) **Sampling (Sec. 3.2)**: We approximate expectations over $\mathbb{P}_{\text{adv}}^*$ using importance sampling from the current prior; and (2) **Learning (Sec. 3.3)**: We update the parameterized adversary ψ to approximate the theoretical optimum $\mathbb{P}_{\text{adv}}^*$ via preference learning.

Outer loop. With the adversary ψ_{k+1} fixed, the ego updates its policy to maximize the expected return under the induced adversarial distribution using standard RL methods:

$$\theta^{k+1} \leftarrow \arg \max_{\theta^k} J(\pi_\theta^k, \mathcal{P}_{\psi_{k+1}}). \quad (4)$$

Crucially, this general framework is agnostic to the specific RL method used for the ego policy. Since the adversary interacts with the ego solely through generated trajectories, the outer loop supports both on-policy and off-policy algorithms, by adjusting the synchronization schedule between the two. Moreover, ADV-0 can be applied to π_θ either outputs continuous control signals (e.g., acceleration) or future trajectory plans (e.g., multi-modal trajectories with scores).

Training proceeds by fixing one player while updating the other. This coupled iteration ensures that the attacker dynamically tracks the defender’s vulnerability frontier, while the defender learns to generalize against an increasingly sophisticated attacker. See Algorithm 1 for implementation.

3.2. Reward-guided Adversarial Sampling & Alignment

To approximate the optimal distribution $\mathbb{P}_{\text{adv}}^*$ without computationally expensive MCMC, we adopt a generate-and-resample paradigm. Instead of generating trajectories from scratch, we sample from a pretrained multi-modal trajectory generator \mathcal{G}_ψ that approximates $\mathbb{P}_{\text{prior}}(\cdot|X)$. Given a context X , the current \mathcal{G}_ψ produces K candidates $\{Y_k^{\text{Adv}}\}_{k=1}^K \sim \mathcal{G}_\psi(\cdot|X)$ with prior probabilities. We then re-weight these candidate to approximate samples from $\mathbb{P}_{\text{adv}}^*$ using GAU.

Direct objective alignment. Prior works (Zhang et al., 2022; 2023) simplify the GAU by assuming a heuristic surrogate, e.g., collision probability. However, this introduces a misalignment: the defender optimizes a comprehensive reward (safety, efficiency, and comfort), while the attacker solely targets collisions. This discrepancy in gradient direction prevents the attacker from identifying non-collision failures (e.g., off-road) and allows the defender to overfit to specific collision modes while remaining vulnerable to other risks. In contrast, ADV-0 directly aligns the GAU

with the defender’s objective by *setting the energy function as the negation of the ego’s cumulative return* (Eq. 3). By targeting exactly what the ego optimizes, the attacker offers holistic supervision signals across the entire reward space, whether they are safety violations or efficiency drops.

Algorithm 1 Closed-Loop Min-Max Policy Optimization

```

1: Input: Initial ego policy  $\pi_\theta$ , Pretrained adversary prior  $\mathcal{G}_{\text{ref}}$ .
2: Hyperparameters: Temperature  $\tau$ , Reward filters  $\delta, \xi$ , Learning rates  $\alpha, \eta$ , Frequency  $N_{\text{freq}}$ , IPL batch size  $M$ .
3: Initialize: Adversary  $\mathcal{G}_\psi \leftarrow \mathcal{G}_{\text{ref}}$ , Ego history buffer  $\mathcal{H}_{\text{ego}} \leftarrow \emptyset$ , Replay buffer  $\mathcal{D}$  (Off-policy) or Batch buffer  $\mathcal{B}$  (On-policy).
4: for timestep  $t = 1$  to  $T_{\text{max}}$  do
5:   // — Phase 1: Adversary Update (Inner Loop) —
6:   if  $t \bmod N_{\text{freq}} == 0$  then
7:     for iteration  $k = 1$  to  $K_{\text{IPL}}$  do
8:       Sample context batch  $\{X_m\}_{m=1}^M$ .
9:       Generate candidates  $\{Y_{m,j}^{\text{Adv}}\}_{j=1}^K \sim \mathcal{G}_\psi(\cdot|X_m), \forall X_m$ .
10:      Calculate  $\{\hat{J}(Y_{m,j}^{\text{Adv}}, \pi_\theta)\}_{j=1}^K$  using  $\mathcal{H}_{\text{ego}}[X_m]$  (Eq. 5).
11:      Construct preference pairs  $\mathcal{D}_{\text{pref}}$  based on all  $\hat{J}$ .
12:      Update  $\psi$  via IPL on  $\mathcal{D}_{\text{pref}}$  (Eq. 8).
13:    end for
14:  end if
15:  // — Phase 2: Ego Update (Outer Loop) —
16:  Sample new scenario context  $X$ .
17:  Generate candidates  $\{Y_k\} \sim \mathcal{G}_\psi(\cdot|X)$ .
18:  Select  $Y^{\text{adv}}$  via softmax sampling (Eq. 6).
19:  Rollout  $\pi_\theta$  in environment  $\mathcal{P}_\psi$  to get  $Y^{\text{Ego}}$ .
20:  Update history:  $\mathcal{H}_{\text{ego}}[X] \leftarrow \text{FIFO}(\mathcal{H}_{\text{ego}} \cup \{Y^{\text{Ego}}\})$ .
21:  if Algorithm is On-Policy (e.g., PPO) then
22:    Store  $Y^{\text{Ego}}$  in Batch Buffer  $\mathcal{B}$ .
23:    if  $\mathcal{B}$  is full then
24:      Update  $\theta$  via Eq. 1 several steps on  $\mathcal{B}$ , then clear  $\mathcal{B}$ .
25:    end if
26:  else if Algorithm is Off-Policy (e.g., SAC) then
27:    Store transitions from  $Y^{\text{Ego}}$  into Replay Buffer  $\mathcal{D}$ .
28:    Sample mini-batch from  $\mathcal{D}$  and update  $\theta$  one step (Eq. 1).
29:  end if
30: end for
    
```

Efficient return estimation. Evaluating the exact return $\mathbb{E}[J(\pi_\theta, Y_k^{\text{Adv}})]$ for all K candidates via closed-loop simulation requires fully rolling out the policy, which is computationally prohibitive. To address this, we propose a *Proxy Reward Evaluator* that estimates the expected return using a lightweight function query. Recognizing that the ego’s response to Y^{Adv} is stochastic (exploration noise) during training, we treat J as a random variable. We maintain a context-aware dynamic buffer of the ego’s recent responses $\mathcal{H}_{\text{ego}}(X) = \{Y_i^{\text{Ego}}|X\}_{i=1}^N$ containing the N most recent trajectories generated by π_θ in context X . For a new context with an empty buffer, we perform a single warm-up rollout using π_θ against the replay log to initialize the buffer. We treat \mathcal{H}_{ego} as an empirical approximation of the current policy distribution. The expected return for a candidate Y_k^{Adv} is estimated via Monte Carlo integration against the history:

$$\hat{J}(Y_k^{\text{Adv}}, \pi_\theta) \approx \frac{1}{N} \sum_{Y_i^{\text{Ego}} \in \mathcal{H}_{\text{ego}}} \mathcal{R}_{\text{proxy}}(Y_i^{\text{Ego}}, Y_k^{\text{Adv}}), \quad (5)$$

where $\mathcal{R}_{\text{proxy}}$ is a vectorized function that computes geometric interactions (e.g., progress, collision overlap) between the adversary path and the cached ego paths without stepping the physics engine. This rule-based proxy provides an efficient and sufficiently accurate gradient direction for adversarial sampling (see Section D.2.1 for implementation).

Temperature-scaled sampling. Finally, to select the adversarial trajectory for training, we implement the Gibbs distribution (Eq. 3) over the finite set of K candidates. The probability of selecting candidate k is given by the scaled softmax distribution over negative estimated returns:

$$\mathbb{P}(Y_k^{\text{Adv}}) = \frac{\exp\left(-\hat{J}(Y_k^{\text{Adv}}, \pi_\theta)/\tau\right)}{\sum_{j=1}^K \exp\left(-\hat{J}(Y_j^{\text{Adv}}, \pi_\theta)/\tau\right)}. \quad (6)$$

This serves as an *importance sampling* step, re-weighting the proposal distribution \mathcal{G}_ψ towards the theoretical optimum $\mathbb{P}_{\text{adv}}^*$ (see Appendix B.1). τ balances exploration and exploitation: $\tau \rightarrow 0$ selects the worst case, while larger τ retains diversity from the prior. It ensures that the defender is exposed to a diverse range of challenging scenarios from the long tail, rather than collapsing into a single worst case.

3.3. Iterative Preference Learning in the Long Tail

While the sampling strategy in Section 3.2 identifies hard cases within the support of \mathcal{G}_ψ , this fixed proposal bounds its efficacy. As the defender π_θ improves, its weakness shifts into the long tail where the prior \mathcal{G}_{ref} has negligible mass. Relying solely on static sampling becomes inefficient. To track the shifting frontier, we update ψ to match the distribution of the generator \mathcal{G}_ψ and the optimal target $\mathbb{P}_{\text{adv}}^*$.

Implicit reward optimization via preferences. Formally, our goal is to minimize the KL-divergence between \mathcal{G}_ψ and $\mathbb{P}_{\text{adv}}^*$. Recall the definition in Eq. 3, we have:

$$\begin{aligned} \min_{\psi} \mathbb{D}_{\text{KL}}(\mathcal{G}_\psi || \mathbb{P}_{\text{adv}}^*) &= \min_{\psi} \mathbb{E}_{Y \sim \mathcal{G}_\psi} [\log \mathcal{G}_\psi(Y|X) / \mathbb{P}_{\text{adv}}^*(Y|X)] \\ &= \min_{\psi} \mathbb{E}_{Y \sim \mathcal{G}_\psi} \left[\log \frac{\mathcal{G}_\psi(Y|X)}{\mathcal{G}_{\text{ref}}(Y|X)} + \frac{1}{\tau} J(\pi_\theta, Y) \right] + \text{const.} \\ &\iff \max_{\psi} \mathbb{E}_{Y \sim \mathcal{G}_\psi} \left[-J(\pi_\theta, Y) - \tau \mathbb{D}_{\text{KL}}(\mathcal{G}_\psi || \mathcal{G}_{\text{ref}}) \right]. \end{aligned} \quad (7)$$

Eq. 7 reveals a standard RL objective: maximizing the expected adversarial reward subject to a KL-divergence constraint. However, directly solving it via policy gradient is notoriously unstable in this context due to the high variance of gradients. The action space of continuous trajectories is high-dimensional, and the zero-sum interaction often leads to mode collapse. Instead of explicit RL, we cast the problem as preference learning. Following Rafailov et al. (2023), the optimal policy for the KL-constrained objective satisfies a specific preference ordering, which is equivalent to optimizing an *implicit reward*. This allows us to update ψ using a supervised loss on preference pairs, bypassing the need for an explicit value function or unstable reward maximization.

Online iterative evolution. Standard preference learning methods are often offline with static preference datasets. Instead, ADV-0 operates in a nonstationary game where the preference labels depend on evolving players. Therefore, we propose online *Iterative Preference Learning* (IPL) in the inner loop. IPL generates preference data on-the-fly, conditioning on the current attacker and labels it using the current defender. This process proceeds on-policy: **(1) Sampling:** For a given context X , a series of candidates are generated $\{Y_k^{\text{Adv}}\}_{k=1}^K$ from the *current* attacker \mathcal{G}_ψ . **(2) Labeling:** Each candidate is evaluated using the proxy reward evaluator $\hat{J}(\cdot, \pi_\theta)$. Crucially, this evaluation uses the *latest* history of the defender. **(3) Pairing:** A preference dataset $\mathcal{D}_{\text{pref}}$ is curated by pairing (Y_w, Y_l) from the candidates, where Y_w is preferred over Y_l if $\hat{J}(Y_w, \pi_\theta) < \hat{J}(Y_l, \pi_\theta)$. To prevent trivial comparisons, we apply a reward margin δ and a spatial diversity filter ξ : $\mathcal{D}_{\text{pref}} = \{(Y_w, Y_l) \mid \hat{J}(Y_l) - \hat{J}(Y_w) > \delta \wedge \|Y_w - Y_l\|_2 > \xi\}$. This reduces noise in the proxy, making preferences distinguishable between structurally different attacks.

Objective. We update the adversarial policy \mathcal{G}_ψ by minimizing the negative log-likelihood of the preferred trajectories. To handle the high variance of heterogeneous traffic scenarios without the high cost of a massive replay buffer, we employ a streaming gradient accumulation strategy to stabilize the training. We process a stream of scenarios sequentially, accumulating gradients over a mini-batch of M scenarios before performing a parameter update. The loss function $\mathcal{L}_{\text{IPL}}(\mathcal{G}_\psi)$ for a mini-batch \mathcal{B} of generated pairs is:

$$\frac{-1}{|\mathcal{B}|} \sum_{(Y_w, Y_l) \in \mathcal{B}} \log \sigma \left(\tau \left[\log \frac{\mathcal{G}_\psi(Y_w|X)}{\mathcal{G}_{\text{ref}}(Y_w|X)} - \log \frac{\mathcal{G}_\psi(Y_l|X)}{\mathcal{G}_{\text{ref}}(Y_l|X)} \right] \right). \quad (8)$$

This reduces the variance of per-scenario update while maintaining the on-policy nature of data generation. Here, the reference model \mathcal{G}_{ref} remains frozen as the pretrained prior.

This streaming evolution ensures that the adversary continuously adapts to the defender’s evolving capabilities. By pushing the generator’s distribution towards the theoretical Gibbs optimum $\mathbb{P}_{\text{adv}}^*$, the defender is continuously trained against the most pertinent long-tail risks, effectively mitigating the distribution shift and forcing robust generalization.

3.4. Theoretical Analysis

We provide a theoretical analysis of the convergence properties of ADV-0 and establish a generalization bound that certifies the agent’s performance in real-world long-tail distributions. Derivations and proofs are provided in Section B.

Convergence to Nash Equilibrium. The interaction between the defender and the attacker is modeled as a regularized zero-sum Markov game. Building on the finding that optimizing Eq. 8 recovers the optimal adversary solved for a Gibbs distribution, we prove that iterative updates constitute

a contraction mapping on the value function space.

Theorem 3.1 (Convergence to Nash Equilibrium). *The iterative updates in ADV-0 converge to a unique fixed point corresponding to the Nash Equilibrium (π^*, ψ^*) of the game. This point satisfies the saddle-point inequality $\mathcal{J}_\tau(\pi, \mathcal{G}_{\psi^*}) \leq \mathcal{J}_\tau(\pi^*, \mathcal{G}_{\psi^*}) \leq \mathcal{J}_\tau(\pi^*, \mathcal{G}_\psi)$ for all feasible policies, where \mathcal{J}_τ is the regularized objective.*

Generalization to real-world long tail. A core concern is whether robustness against a generated adversary \mathcal{P}_ψ translates to safety in the real-world long-tail distribution $\mathcal{P}_{\text{real}}$. We model the real dynamics as an unknown distribution lying within the trust region of the traffic prior. We derive a certified lower bound on the expected return by measuring the discrepancy between two induced transition dynamics.

Theorem 3.2 (Generalizability). *Let V_{max} be the maximum of the value function, $\mathcal{P}_{\text{real}}$ be the real dynamics, and π_θ is trained under the adversarial dynamics \mathcal{P}_ψ induced by \mathcal{G}_ψ . The performance of π_θ under $\mathcal{P}_{\text{real}}$ is bounded by:*

$$J(\pi_\theta, \mathcal{P}_{\text{real}}) \geq J(\pi_\theta, \mathcal{P}_\psi) - \frac{\gamma V_{\text{max}} \sqrt{2}}{1 - \gamma} \sqrt{\mathbb{E}[D_{\text{KL}}(\mathcal{G}_\psi \| \mathcal{G}_{\text{ref}})]}.$$

Theorem 3.2 implies that optimizing against the generated adversary maximizes a certified lower bound on the expected return in the real world. The outer loop maximizes the robust return $J(\pi_\theta, \mathcal{P}_\psi)$, while the inner loop minimizes the KL-divergence, ensuring that safety improvements in the adversarial domain transfer to open-world deployment.

4. Experiments

We empirically evaluate ADV-0 to answer three core questions: (1) Can ADV-0 generate plausible yet long-tailed scenarios that effectively expose the vulnerabilities of driving agents? (2) Does the training process yield a robust policy that generalizes to diverse adversarial attacks? (3) Can the safety improvements observed in simulation transfer to real-world long-tailed events? All experiments are performed in MetaDrive simulator based on the WOMD.

4.1. Generating Safety-Critical Scenarios

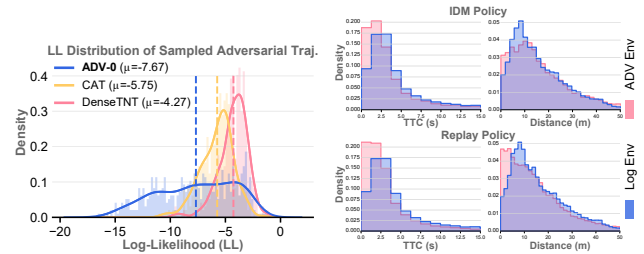


Figure 2. LL distribution of different adversarial generators.

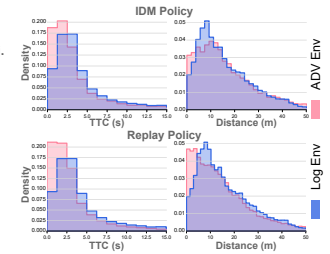


Figure 3. Scene-level distributions of B2B distance and TTC.

Main results. We first evaluate ADV-0 in generating safety-critical scenarios against various ego policies. As presented in Table 1, ADV-0 consistently outperforms competing baselines in exposing system vulnerabilities, espe-

cially for reactive policies such as IDM and RL. A detailed ablation in Table 6 further highlights two findings: (1) The proposed energy-based sampling strategy (Eq. 6) is effective compared to the standard logit-based scheme. (2) IPL-based fine-tuning, which is insensitive to RL, further refines the adversary. By fine-tuning the generator against specific ego policies, the adversary learns to exploit specific weaknesses.

Table 1. Safety-critical scenario generation. *CR* denotes the collision rate of the ego in generated scenarios, and *ER* denotes the ego’s cumulative return. Ego is controlled by Replay, IDM, and trained PPO policies, respectively. Metrics of ADV-0 are mean values across all training methods. See full results in Table 6.

Adversary	Replay		IDM		RL Agent	
	CR \uparrow	ER \downarrow	CR \uparrow	ER \downarrow	CR \uparrow	ER \downarrow
Replay	-	-	19.03%	51.75	16.80%	51.65
Heuristic	100.00%	0.00	74.70%	32.12	69.64%	24.90
CAT	90.08%	1.03	43.13%	43.47	36.84%	42.26
KING	23.28%	47.67	24.49%	49.41	21.26%	49.32
AdvTrajOpt	69.64%	3.12	26.92%	45.36	28.95%	45.10
GOOSE	20.46%	48.52	24.48%	49.45	13.88%	51.80
SAGE	74.53%	2.57	36.50%	43.81	35.40%	42.87
SEAL	59.06%	8.58	36.70%	43.75	37.63%	41.99
ADV-0 (ours)	91.10%	0.99	45.83%	40.03	40.68%	39.13

Distribution of the long tail. ADV-0 can navigate the long-tail distribution of scenarios. Figure 2 illustrates the log-likelihood (LL) distribution of the sampled adversarial trajectories. Compared to CAT and pretrained prior, the distribution of ADV-0 is shifted towards lower likelihood and exhibits a wider variance. This indicates that it uncovers rare but plausible, *behavior-level* events that are typically ignored by standard priors. Figure 3 shows the *scene-level* statistics. ADV-0 produces notably lower Time-to-Collision (TTC) and closer Bumper-to-Bumper (B2B) distances compared to the naturalistic data. Crucially, this aggressiveness does not compromise physical plausibility. As shown in Figure 9, ADV-0 maintains a comparable realism penalty.

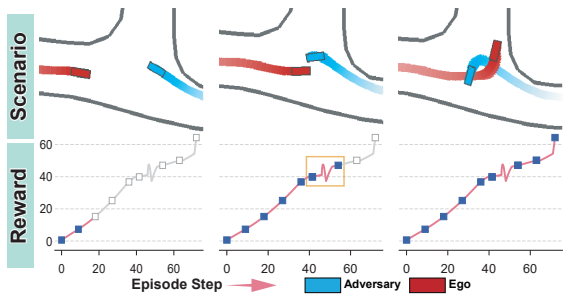


Figure 4. Examples of generated reward-reduced adversarial scenarios from ADV-0. Additional cases are shown in Figure 15.

Beyond collision. ADV-0 directly targets the ego’s return, allowing for the discovery of diverse failure modes beyond crashes. As shown in Figure 4 and Figure 15, the adversary can force the ego into abnormal behaviors and non-collision failures, such as stalling at intersections or deviating from

reference paths. These behaviors result in a drastic drop in accumulated reward (e.g., lack of progress or discomfort penalties) even if a collision is avoided, which are critical performance risks often ignored by collision-centric attacks.

Table 2. Performance validation of learned policies. Results are averaged across 6 RL methods (GRPO, PPO, PPO-Lag, SAC, SAC-Lag, TD3). This table compares the performances of agents learned by different adversarial methods and evaluate on different generated scenarios. Full results are shown in Tables 7, 8, 9, 10, 11, 12.

	Val. Env.	RC \uparrow	Crash \downarrow	Reward \uparrow	Cost \downarrow
ADV-0 (w/ IPL)	Replay	0.742 \pm 0.011	0.159 \pm 0.019	49.56 \pm 1.05	0.480 \pm 0.013
	ADV-0	0.695 \pm 0.011	0.289 \pm 0.029	44.60 \pm 0.83	0.598 \pm 0.022
	CAT	0.704 \pm 0.011	0.271 \pm 0.025	45.68 \pm 1.16	0.585 \pm 0.025
	SAGE	0.699 \pm 0.013	0.263 \pm 0.025	45.19 \pm 1.54	0.567 \pm 0.028
	Heuristic	0.710 \pm 0.016	0.217 \pm 0.021	45.41 \pm 2.08	0.552 \pm 0.035
	Avg.	0.710 \pm 0.012	0.240 \pm 0.024	46.09 \pm 1.33	0.556 \pm 0.027
ADV-0 (w/o IPL)	Replay	0.719 \pm 0.020	0.167 \pm 0.024	46.41 \pm 1.97	0.540 \pm 0.023
	ADV-0	0.664 \pm 0.018	0.317 \pm 0.030	41.03 \pm 1.87	0.657 \pm 0.020
	CAT	0.677 \pm 0.017	0.299 \pm 0.035	42.30 \pm 1.68	0.643 \pm 0.030
	SAGE	0.672 \pm 0.024	0.270 \pm 0.028	42.17 \pm 2.38	0.610 \pm 0.038
	Heuristic	0.679 \pm 0.022	0.239 \pm 0.041	41.78 \pm 2.08	0.612 \pm 0.040
	Avg.	0.683 \pm 0.020	0.258 \pm 0.031	42.74 \pm 2.00	0.613 \pm 0.030
CAT	Replay	0.720 \pm 0.014	0.183 \pm 0.026	46.52 \pm 1.15	0.528 \pm 0.015
	ADV-0	0.660 \pm 0.018	0.332 \pm 0.043	40.70 \pm 0.97	0.660 \pm 0.020
	CAT	0.667 \pm 0.017	0.313 \pm 0.032	41.30 \pm 1.48	0.652 \pm 0.018
	SAGE	0.660 \pm 0.021	0.307 \pm 0.025	41.41 \pm 2.09	0.628 \pm 0.017
	Heuristic	0.676 \pm 0.021	0.261 \pm 0.034	41.72 \pm 1.69	0.605 \pm 0.023
	Avg.	0.676 \pm 0.018	0.279 \pm 0.032	42.33 \pm 1.47	0.614 \pm 0.019
Heuristic	Replay	0.682 \pm 0.032	0.201 \pm 0.018	42.75 \pm 3.04	0.592 \pm 0.037
	ADV-0	0.637 \pm 0.047	0.331 \pm 0.021	39.09 \pm 2.12	0.678 \pm 0.028
	CAT	0.650 \pm 0.021	0.311 \pm 0.020	40.11 \pm 2.38	0.668 \pm 0.033
	SAGE	0.642 \pm 0.042	0.314 \pm 0.019	39.53 \pm 2.58	0.658 \pm 0.025
	Heuristic	0.641 \pm 0.030	0.279 \pm 0.016	38.81 \pm 2.61	0.655 \pm 0.028
	Avg.	0.650 \pm 0.034	0.287 \pm 0.019	40.06 \pm 2.54	0.649 \pm 0.032
Replay	Replay	0.692 \pm 0.035	0.209 \pm 0.030	42.93 \pm 1.32	0.588 \pm 0.025
	ADV-0	0.622 \pm 0.038	0.374 \pm 0.038	36.80 \pm 2.48	0.700 \pm 0.020
	CAT	0.642 \pm 0.040	0.368 \pm 0.037	38.26 \pm 1.83	0.683 \pm 0.030
	SAGE	0.625 \pm 0.040	0.339 \pm 0.040	37.68 \pm 1.84	0.660 \pm 0.032
	Heuristic	0.638 \pm 0.031	0.310 \pm 0.034	37.80 \pm 2.41	0.672 \pm 0.015
	Avg.	0.644 \pm 0.037	0.320 \pm 0.036	38.70 \pm 1.97	0.661 \pm 0.028

4.2. Learning Generalizable Driving Policies

Generalization to unseen adversaries. A core challenge in adversarial RL is overfitting to a specific adversary, which limits generalization to unseen risks. We conduct a cross-validation where agents trained via different methods are tested across a spectrum of environments. Table 2 reports the performance averaged across six RL algorithms. We observe that agents trained with ADV-0 (w/ IPL) consistently achieve the best results across all metrics. While baselines often perform well against their own attacks, they degrade when applied to unseen adversarial distributions. In contrast, ADV-0 maintains consistent generalizability. The comparison between ADV-0 (w/o IPL) and CAT indicates the benefit of directly aligning the GAU with the ego’s objective. By actively exploring the long tail via IPL, ADV-0 enables generalized robustness to handle unseen risks.

Impact of IPL. To isolate the gain provided by IPL, we compare the performance of agents and adversaries trained with and without IPL in Table 3. The inclusion of IPL in the adversary creates a more challenging environment, evidenced by the drop in agent rewards. However, the agent trained with full ADV-0 becomes more robust when facing the stronger adversary. This confirms that the dynamic evolution of the adversary via IPL forces the defender to cover broader vulnerabilities. Qualitative evidence of this dynamic evolution is shown in Figure 13. Finally, we study the sample efficiency and overfitting risks regarding the training budget. As shown in Figure 5, the gap between training and testing performance narrows with IPL, indicating that active discovery of diverse failures effectively mitigates the risk of overfitting to limited training data. Detailed learning curves and results are provided in Figures 10-11 and Tables 7-12.

Table 3. **Cross-validation of ADV-0.** Performances of agents and adversaries with/without IPL. Decrease indicates the percentage change in performance when facing an IPL-enhanced adversary compared to the baseline. Improvement indicates the percentage change when the agent is trained with IPL compared to the other.

Agent/Adversary	Reward (\uparrow)		
	Adversary (w/o IPL)	Adversary (w/ IPL)	Decrease
Agent w/o IPL	41.03 \pm 1.87	39.01 \pm 0.97	-4.92%
Agent w/ IPL	44.60 \pm 0.83	43.47 \pm 1.40	-2.53%
Improvement	+8.70%	+11.43%	
Agent/Adversary	Cost (\downarrow)		
	Adversary (w/o IPL)	Adversary (w/ IPL)	Decrease
Agent w/o IPL	0.657 \pm 0.020	0.685 \pm 0.016	+4.26%
Agent w/ IPL	0.598 \pm 0.022	0.615 \pm 0.025	+2.84%
Improvement	-8.98%	-10.22%	-

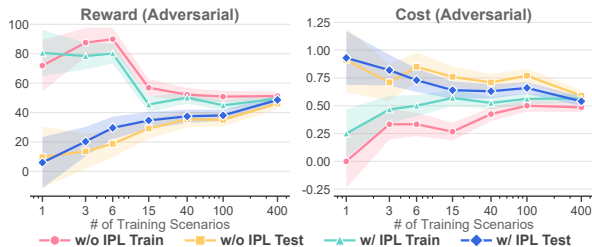


Figure 5. Generalization gap over different training budgets.

4.3. Improving Policy Robustness in the Long Tail

Main results. While ADV-0 has presented robustness against generated adversaries, it is crucial to verify whether this performance generalizes to real-world, naturally occurring long-tail events. To this end, we curate unbiased held-out sets mined from real-world WOMB logs, including only high-risk scenarios categorized by extreme safety criticality (e.g., critical TTC, PET) and semantic rarity (e.g., rare behaviors). As shown in Table 4 (detailed in Table 15),

agents trained via ADV-0 demonstrate superior zero-shot robustness compared to baselines. It achieves the highest safety margins and stability scores, significantly reducing the rates of near misses and RDP violations, indicating that the agent learns to anticipate risks before they become critical, rather than merely reacting to emergencies. Examples in Figures 6 and 14 further visualize these defensive behaviors: ADV-0 agent proactively yields to aggressive cut-ins and navigates sudden occlusions where baseline agents fail.

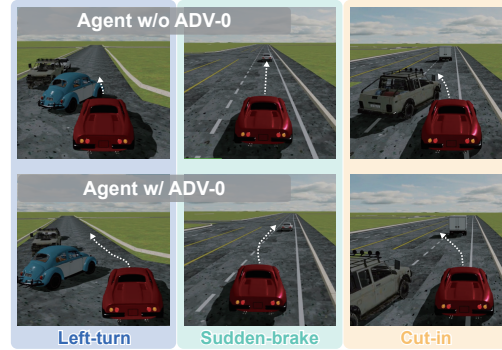


Figure 6. Visualization of improved safe driving ability after being trained with ADV-0. More examples are shown in Figure 14.

4.4. Algorithmic Analysis

Applications to motion planners. To show the generality of ADV-0, we extend our evaluation beyond RL agents to two kinds of SOTA learning-based trajectory planners: PlanTF (Cheng et al., 2024) (multimodal scoring) and SMART (Wu et al., 2024) (autoregressive generation). As shown in Tables 5 and 13, adversarial fine-tuning via ADV-0 yields consistent improvements for both architectures. We further analyze the internal behavior of the planners using the trajectory-level breakdown in Table 14. The results indicate that fine-tuned models learn to prioritize safety constraints significantly more than pretrained priors. This safety improvement comes with a trade-off in efficiency. Interestingly, we observe that the performance of these planners remains slightly lower than RL agents discussed previously. We attribute this to two factors: (1) the covariate shift in behavior cloning models (Karkus et al., 2025), where they struggle to recover when the adversary forces it into out-of-distribution states; and (2) the latency introduced by the re-planning horizon. Unlike end-to-end RL policies that output immediate control actions, they generate a future trajectory executed by a controller. This delayed reaction limits the ability to react instantaneously to aggressive attacks.

Impact of temperature parameter. We study the sensitivity of the sampling temperature τ in Eq. 6, which modulates the trade-off between adversarial exploitation and exploration. Figure 7 illustrates an obvious trade-off: (1) At extremely low temperatures ($\tau \rightarrow 0$), the sampling degenerates into a deterministic hard mode. This leads to sub-optimal performance, likely because an overly aggressive

Table 4. **Robustness on mined real-world long-tailed sets.** Average agent performance on four long-tail scenario categories filtered by criteria: *Critical TTC* (min TTC < 0.4s), *Critical PET* (PET < 1.0s), *Hard Dynamics* (Acc. < -4.0m/s² or |Jerk| > 4.0m/s³), and *Rare Cluster* (topologically sparse trajectory clusters). Metrics assess average *Safety Margin* (higher values indicate earlier risk detection), *Stability & Comfort* (lower Jerk indicates smoother control), and *Defensive Driving*, quantified by Near-Miss Rate (proximity without collision) and RDP Violation (percentage of time requiring deceleration > 6m/s² to avoid collision). Full results are shown in Table 15.

	Reactive Traffic	Safety Margin		Stability & Comfort		Defensive Driving	
		Avg Min-TTC (↑)	Avg Min-PET (↑)	Mean Abs Jerk (↓)	95% Jerk (↓)	Near-Miss Rate (↓)	RDP Violation Rate (↓)
ADV-0 (w/ IPL)	✓	0.993 ± 0.189	1.150 ± 0.317	1.653 ± 0.169	5.053 ± 0.885	63.45% ± 4.34%	33.70% ± 3.77%
	✗	1.527 ± 0.182	1.103 ± 0.313	1.617 ± 0.204	5.177 ± 0.953	60.97% ± 3.94%	36.45% ± 2.85%
CAT	✓	0.825 ± 0.192	1.017 ± 0.317	1.875 ± 0.229	5.422 ± 0.833	83.04% ± 5.99%	44.80% ± 6.12%
	✗	1.415 ± 0.462	0.980 ± 0.327	1.979 ± 0.193	6.002 ± 0.931	75.36% ± 7.86%	51.20% ± 4.74%
Heuristic	✓	0.864 ± 0.200	1.150 ± 0.467	2.129 ± 0.237	6.542 ± 0.942	74.46% ± 5.98%	48.79% ± 3.65%
	✗	1.601 ± 0.538	1.093 ± 0.450	2.199 ± 0.218	6.778 ± 1.066	68.82% ± 9.05%	52.10% ± 1.77%
Replay	✓	0.587 ± 0.185	0.683 ± 0.217	2.779 ± 0.431	8.265 ± 1.718	89.53% ± 4.30%	69.73% ± 5.27%
	✗	0.978 ± 0.462	0.730 ± 0.233	2.720 ± 0.383	8.104 ± 1.537	85.13% ± 4.58%	68.50% ± 4.68%

Table 5. **Application to learning-based planners.** Performance comparisons of two SOTA trajectory planning models before and after fine-tuning using ADV-0 (GRPO). See Table 13 for details.

Model	RC ↑	Crash ↓	Reward ↑	Cost ↓
PlanTF	0.628 ± 0.025	0.357 ± 0.031	35.85 ± 2.51	1.04 ± 0.04
+ ADV-0	0.674 ± 0.016	0.263 ± 0.025	41.98 ± 1.62	0.77 ± 0.02
Rel. Change	+7.46%	-26.23%	+17.11%	-25.68%
SMART	0.587 ± 0.029	0.396 ± 0.034	32.66 ± 2.85	1.15 ± 0.05
+ ADV-0	0.631 ± 0.015	0.305 ± 0.023	37.85 ± 1.70	0.92 ± 0.02
Rel. Change	+7.57%	-22.88%	+15.86%	-20.31%

attacker overwhelms the defender early in training, without learning generalized robustness. (2) Conversely, high values ($\tau = 5.0$) reduce the adversarial signal, degrading ADV-0 to domain randomization. The attacker fails to consistently expose weaknesses. The results indicate that a moderate value ($\tau = 0.1$) achieves the best balance. It introduces sufficient stochasticity to cover diverse long-tail distribution while maintaining enough focus to prioritize high-risk regions, effectively forming an automatic regularization.

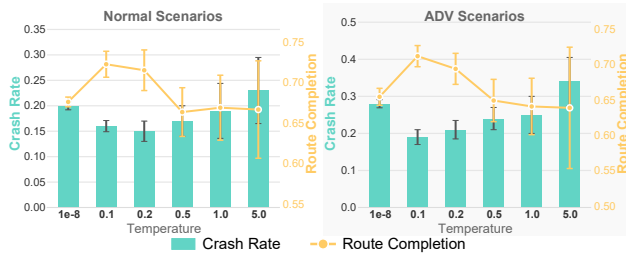


Figure 7. Impacts of the temperature parameter in sampling.

Ablation on return estimator. The inner loop relies on the quality of the return estimator \hat{J} used to label preferences. We compare our rule-based proxy against three baselines: *GTReward* (oracle simulation), *Experience* (retrieval from history), and *RewardModel* (learnable neural network). Figure 8 reports the IPL training curves. Surpris-

ingly, the rule-based proxy achieves low and stable preference loss comparable to the oracle, outperforming other estimators. Figure 12 measures a strong Spearman correlation of $\rho = 0.77$ between the proxy estimates and oracle returns. This suggests that the geometric proxy provides a high-fidelity and low-variance ranking signal, which is sufficient for adversarial sampling. Future work may explore using the Q-network from an Actor-Critic architecture for value estimation to handle more complex interactions.

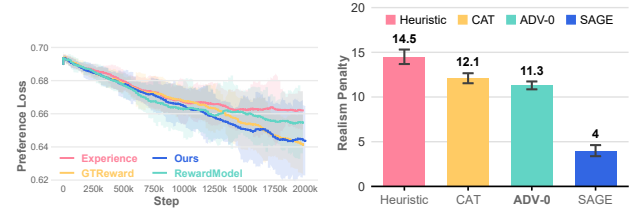


Figure 8. Impacts of different preference loss estimators. Figure 9. Realism penalty value of different adversarial methods.

5. Conclusion

This paper presents ADV-0, a closed-loop min-max policy optimization framework designed to enhance the robustness of AD models against long-tail risks. By formulating the problem as a zero-sum game and solving it via an alternating end-to-end training pipeline, we bridge the gap between adversarial generation and robust policy learning. We theoretically proved that it converges to a Nash Equilibrium and maximizes a certified lower bound. Empirical results suggest that ADV-0 not only generates effective safety-critical scenarios but also improves the generalizability of both RL agents and motion planners against diverse long-tail risks. Despite the promising results, several limitations exist. (1) The reliance on high-fidelity simulators for online RL training limits scalability. (2) Extending ADV-0 to vision-based sensor inputs may require differentiable neural rendering, which remains a non-trivial challenge. Future work could explore offline RL techniques (Karkus et al., 2025) to improve training efficiency and vision-based adversarial generation.

Impact Statement

This paper presents work whose goal is to advance the field of Machine Learning, specifically in the domain of safety-critical autonomous systems. Our research focuses on identifying system vulnerabilities and improving robustness against rare, long-tail events, which is a prerequisite for the safe large-scale deployment of autonomous vehicles. By providing a rigorous framework for generating and mitigating high-risk scenarios, this work contributes to reducing potential accidents and enhancing public trust in automation technologies. While adversarial generation techniques could theoretically be repurposed to identify vulnerabilities for malicious intent, our framework is designed as a defensive mechanism to patch these flaws before deployment. We do not identify any specific negative ethical consequences or societal risks associated with this research, as the adversarial generation is strictly confined to simulation environments for the purpose of system validation and improvement.

References

- Achiam, J., Held, D., Tamar, A., and Abbeel, P. Constrained policy optimization. In *International conference on machine learning*, pp. 22–31. PMLR, 2017.
- Amirkhani, A., Karimi, M. P., and Banitalebi-Dehkordi, A. A survey on adversarial attacks and defenses for object detection and their applications in autonomous vehicles. *The Visual Computer*, 39(11):5293–5307, 2023.
- Anzalone, L., Barra, P., Barra, S., Castiglione, A., and Nappi, M. An end-to-end curriculum learning approach for autonomous driving scenarios. *IEEE Transactions on Intelligent Transportation Systems*, 23(10):19817–19826, 2022.
- Bolloor, A., He, X., Gill, C., Vorobeychik, Y., and Zhang, X. Simple physical adversarial examples against end-to-end autonomous driving models. In *2019 IEEE International Conference on Embedded Software and Systems (ICES)*, pp. 1–7. IEEE, 2019.
- Brunke, L., Greeff, M., Hall, A. W., Yuan, Z., Zhou, S., Panerati, J., and Schoellig, A. P. Safe learning in robotics: From learning-based control to safe reinforcement learning. *Annual Review of Control, Robotics, and Autonomous Systems*, 5(1):411–444, 2022.
- Chen, J., Yuan, B., and Tomizuka, M. Model-free deep reinforcement learning for urban autonomous driving. In *2019 IEEE intelligent transportation systems conference (ITSC)*, pp. 2765–2771. IEEE, 2019.
- Chen, K., Sun, W., Cheng, H., and Zheng, S. Rift: Closed-loop rl fine-tuning for realistic and controllable traffic simulation. *arXiv preprint arXiv:2505.03344*, 2025.
- Chen, L., Wu, P., Chitta, K., Jaeger, B., Geiger, A., and Li, H. End-to-end autonomous driving: Challenges and frontiers. *IEEE Transactions on Pattern Analysis and Machine Intelligence*, 2024.
- Cheng, J., Chen, Y., Mei, X., Yang, B., Li, B., and Liu, M. Rethinking imitation-based planners for autonomous driving. In *2024 IEEE International Conference on Robotics and Automation (ICRA)*, pp. 14123–14130. IEEE, 2024.
- Deng, Y., Zhang, T., Lou, G., Zheng, X., Jin, J., and Han, Q.-L. Deep learning-based autonomous driving systems: A survey of attacks and defenses. *IEEE Transactions on Industrial Informatics*, 17(12):7897–7912, 2021.
- Ding, W., Chen, B., Xu, M., and Zhao, D. Learning to collide: An adaptive safety-critical scenarios generating method. In *2020 IEEE/RSJ International Conference on Intelligent Robots and Systems (IROS)*, pp. 2243–2250. IEEE, 2020.
- Ding, W., Xu, C., Arief, M., Lin, H., Li, B., and Zhao, D. A survey on safety-critical driving scenario generation—a methodological perspective. *IEEE Transactions on Intelligent Transportation Systems*, 24(7):6971–6988, 2023.
- Fang, S., Cui, Y., Liang, H., Lv, C., Hang, P., and Sun, J. Corevla: A dual-stage end-to-end autonomous driving framework for long-tail scenarios via collect-and-refine. *arXiv preprint arXiv:2509.15968*, 2025.
- Feng, S., Yan, X., Sun, H., Feng, Y., and Liu, H. X. Intelligent driving intelligence test for autonomous vehicles with naturalistic and adversarial environment. *Nature communications*, 12(1):748, 2021.
- Feng, S., Sun, H., Yan, X., Zhu, H., Zou, Z., Shen, S., and Liu, H. X. Dense reinforcement learning for safety validation of autonomous vehicles. *Nature*, 615(7953):620–627, 2023.
- Gu, J., Sun, C., and Zhao, H. Densentnt: End-to-end trajectory prediction from dense goal sets. In *Proceedings of the IEEE/CVF international conference on computer vision*, pp. 15303–15312, 2021.
- Guo, D., Yang, D., Zhang, H., Song, J., Zhang, R., Xu, R., Zhu, Q., Ma, S., Wang, P., Bi, X., et al. Deepseek-r1: Incentivizing reasoning capability in llms via reinforcement learning. *arXiv preprint arXiv:2501.12948*, 2025.
- Haarnoja, T., Zhou, A., Abbeel, P., and Levine, S. Soft actor-critic: Off-policy maximum entropy deep reinforcement learning with a stochastic actor. In *International conference on machine learning*, pp. 1861–1870. Pmlr, 2018.

- Hanselmann, N., Renz, K., Chitta, K., Bhattacharyya, A., and Geiger, A. King: Generating safety-critical driving scenarios for robust imitation via kinematics gradients. In *European Conference on Computer Vision*, pp. 335–352. Springer, 2022.
- He, X., Yang, H., Hu, Z., and Lv, C. Robust lane change decision making for autonomous vehicles: An observation adversarial reinforcement learning approach. *IEEE Transactions on Intelligent Vehicles*, 8(1):184–193, 2022.
- Isele, D., Rahimi, R., Cosgun, A., Subramanian, K., and Fujimura, K. Navigating occluded intersections with autonomous vehicles using deep reinforcement learning. In *2018 IEEE international conference on robotics and automation (ICRA)*, pp. 2034–2039. IEEE, 2018.
- Jiang, B., Chen, S., Zhang, Q., Liu, W., and Wang, X. Al-phadrive: Unleashing the power of vlms in autonomous driving via reinforcement learning and reasoning. *arXiv preprint arXiv:2503.07608*, 2025.
- Kamalaruban, P., Huang, Y.-T., Hsieh, Y.-P., Rolland, P., Shi, C., and Cevher, V. Robust reinforcement learning via adversarial training with langevin dynamics. *Advances in Neural Information Processing Systems*, 33:8127–8138, 2020.
- Karkus, P., Igl, M., Chen, Y., Chitta, K., Packer, J., Douillard, B., Tian, R., Naumann, A., Garcia-Cobo, G., Tan, S., et al. Beyond behavior cloning in autonomous driving: a survey of closed-loop training techniques. *Authorea Preprints*, 2025.
- Kiran, B. R., Sobh, I., Talpaert, V., Mannion, P., Al Salhab, A. A., Yogamani, S., and Pérez, P. Deep reinforcement learning for autonomous driving: A survey. *IEEE transactions on intelligent transportation systems*, 23(6): 4909–4926, 2021.
- Knox, W. B., Allievi, A., Banzhaf, H., Schmitt, F., and Stone, P. Reward (mis) design for autonomous driving. *Artificial Intelligence*, 316:103829, 2023.
- Kuutti, S., Fallah, S., and Bowden, R. Training adversarial agents to exploit weaknesses in deep control policies. In *2020 IEEE International Conference on Robotics and Automation (ICRA)*, pp. 108–114. IEEE, 2020.
- Li, D., Ren, J., Wang, Y., Wen, X., Li, P., Xu, L., Zhan, K., Xia, Z., Jia, P., Lang, X., et al. Finetuning generative trajectory model with reinforcement learning from human feedback. *arXiv preprint arXiv:2503.10434*, 2025a.
- Li, Q., Peng, Z., Feng, L., Zhang, Q., Xue, Z., and Zhou, B. Metadrive: Composing diverse driving scenarios for generalizable reinforcement learning. *IEEE transactions on pattern analysis and machine intelligence*, 45(3):3461–3475, 2022.
- Li, Y., Tian, M., Zhu, D., Zhu, J., Lin, Z., Xiong, Z., and Zhao, X. Drive-r1: Bridging reasoning and planning in vlms for autonomous driving with reinforcement learning. *arXiv preprint arXiv:2506.18234*, 2025b.
- Li, Z., Cao, X., Gao, X., Tian, K., Wu, K., Anis, M., Zhang, H., Long, K., Jiang, J., Li, X., et al. Simulating the unseen: Crash prediction must learn from what did not happen. *arXiv preprint arXiv:2505.21743*, 2025c.
- Liu, H. X. and Feng, S. Curse of rarity for autonomous vehicles. *nature communications*, 15(1):4808, 2024.
- Liu, Y., Peng, Z., Cui, X., and Zhou, B. Adv-bmt: Bidirectional motion transformer for safety-critical traffic scenario generation. *arXiv preprint arXiv:2506.09485*, 2025.
- Luo, Y., Xu, H., Li, Y., Tian, Y., Darrell, T., and Ma, T. Algorithmic framework for model-based deep reinforcement learning with theoretical guarantees. *arXiv preprint arXiv:1807.03858*, 2018.
- Ma, X., Driggs-Campbell, K., and Kochenderfer, M. J. Improved robustness and safety for autonomous vehicle control with adversarial reinforcement learning. In *2018 IEEE Intelligent Vehicles Symposium (IV)*, pp. 1665–1671. IEEE, 2018.
- Mei, Y., Nie, T., Sun, J., and Tian, Y. Bayesian fault injection safety testing for highly automated vehicles with uncertainty. *IEEE Transactions on Intelligent Vehicles*, 2024.
- Mei, Y., Nie, T., Sun, J., and Tian, Y. Llm-attacker: Enhancing closed-loop adversarial scenario generation for autonomous driving with large language models. *arXiv preprint arXiv:2501.15850*, 2025.
- Nie, T., Mei, Y., Tang, Y., He, J., Sun, J., Shi, H., Ma, W., and Sun, J. Steerable adversarial scenario generation through test-time preference alignment. *arXiv preprint arXiv:2509.20102*, 2025.
- Ouyang, L., Wu, J., Jiang, X., Almeida, D., Wainwright, C., Mishkin, P., Zhang, C., Agarwal, S., Slama, K., Ray, A., et al. Training language models to follow instructions with human feedback. *Advances in neural information processing systems*, 35:27730–27744, 2022.
- Pan, X., Seita, D., Gao, Y., and Canny, J. Risk averse robust adversarial reinforcement learning. In *2019 International Conference on Robotics and Automation (ICRA)*, pp. 8522–8528. IEEE, 2019.
- Pinto, L., Davidson, J., Sukthankar, R., and Gupta, A. Robust adversarial reinforcement learning. In *International conference on machine learning*, pp. 2817–2826. PMLR, 2017.

- Rafailov, R., Sharma, A., Mitchell, E., Manning, C. D., Ermon, S., and Finn, C. Direct preference optimization: Your language model is secretly a reward model. *Advances in neural information processing systems*, 36: 53728–53741, 2023.
- Ransiek, J., Plaum, J., Langner, J., and Sax, E. Goose: Goal-conditioned reinforcement learning for safety-critical scenario generation. In *2024 IEEE 27th International Conference on Intelligent Transportation Systems (ITSC)*, pp. 2651–2658. IEEE, 2024.
- Saxena, D. M., Bae, S., Nakhaei, A., Fujimura, K., and Likhachev, M. Driving in dense traffic with model-free reinforcement learning. In *2020 IEEE International Conference on Robotics and Automation (ICRA)*, pp. 5385–5392. IEEE, 2020.
- Scherrer, B. Approximate policy iteration schemes: A comparison. In *International Conference on Machine Learning*, pp. 1314–1322. PMLR, 2014.
- Schulman, J., Wolski, F., Dhariwal, P., Radford, A., and Klimov, O. Proximal policy optimization algorithms. *arXiv preprint arXiv:1707.06347*, 2017.
- Stoler, B., Navarro, I., Francis, J., and Oh, J. Seal: Towards safe autonomous driving via skill-enabled adversary learning for closed-loop scenario generation. *IEEE Robotics and Automation Letters*, 10(9):9320–9327, 2025.
- Tang, Y., Liao, H., Nie, T., He, J., Qu, A., Chen, K., Ma, W., Li, Z., Sun, L., and Xu, C. E3ad: An emotion-aware vision-language-action model for human-centric end-to-end autonomous driving. *arXiv preprint arXiv:2512.04733*, 2025.
- Tessler, C., Efroni, Y., and Mannor, S. Action robust reinforcement learning and applications in continuous control. In *International Conference on Machine Learning*, pp. 6215–6224. PMLR, 2019.
- Tian, K., Mao, J., Zhang, Y., Jiang, J., Zhou, Y., and Tu, Z. Nuscenes-spatialqa: A spatial understanding and reasoning benchmark for vision-language models in autonomous driving. *arXiv preprint arXiv:2504.03164*, 2025.
- Tian, R., Li, B., Weng, X., Chen, Y., Schmerling, E., Wang, Y., Ivanovic, B., and Pavone, M. Tokenize the world into object-level knowledge to address long-tail events in autonomous driving. *arXiv preprint arXiv:2407.00959*, 2024.
- Toromanoff, M., Wirbel, E., and Moutarde, F. End-to-end model-free reinforcement learning for urban driving using implicit affordances. In *Proceedings of the IEEE/CVF conference on computer vision and pattern recognition*, pp. 7153–7162, 2020.
- Tu, J., Ren, M., Manivasagam, S., Liang, M., Yang, B., Du, R., Cheng, F., and Urtasun, R. Physically realizable adversarial examples for lidar object detection. In *Proceedings of the IEEE/CVF conference on computer vision and pattern recognition*, pp. 13716–13725, 2020.
- Tu, J., Li, H., Yan, X., Ren, M., Chen, Y., Liang, M., Bitar, E., Yumer, E., and Urtasun, R. Exploring adversarial robustness of multi-sensor perception systems in self driving. *arXiv preprint arXiv:2101.06784*, 2021.
- Tuncali, C. E., Fainekos, G., Ito, H., and Kapinski, J. Simulation-based adversarial test generation for autonomous vehicles with machine learning components. In *2018 IEEE intelligent vehicles symposium (IV)*, pp. 1555–1562. IEEE, 2018.
- Vinitsky, E., Du, Y., Parvate, K., Jang, K., Abbeel, P., and Bayen, A. Robust reinforcement learning using adversarial populations. *arXiv preprint arXiv:2008.01825*, 2020.
- Wachi, A. Failure-scenario maker for rule-based agent using multi-agent adversarial reinforcement learning and its application to autonomous driving. *arXiv preprint arXiv:1903.10654*, 2019.
- Wang, J., Pun, A., Tu, J., Manivasagam, S., Sadat, A., Casas, S., Ren, M., and Urtasun, R. Advsim: Generating safety-critical scenarios for self-driving vehicles. In *Proceedings of the IEEE/CVF Conference on Computer Vision and Pattern Recognition*, pp. 9909–9918, 2021.
- Wang, Y., Luo, W., Bai, J., Cao, Y., Che, T., Chen, K., Chen, Y., Diamond, J., Ding, Y., Ding, W., et al. Alpamayo-r1: Bridging reasoning and action prediction for generalizable autonomous driving in the long tail. *arXiv preprint arXiv:2511.00088*, 2025a.
- Wang, Y., Xing, S., Can, C., Li, R., Hua, H., Tian, K., Mo, Z., Gao, X., Wu, K., Zhou, S., et al. Generative ai for autonomous driving: Frontiers and opportunities. *arXiv preprint arXiv:2505.08854*, 2025b.
- Wu, W., Feng, X., Gao, Z., and Kan, Y. Smart: Scalable multi-agent real-time motion generation via next-token prediction. *Advances in Neural Information Processing Systems*, 37:114048–114071, 2024.
- Xing, S., Hua, H., Gao, X., Zhu, S., Li, R., Tian, K., Li, X., Huang, H., Yang, T., Wang, Z., et al. Autotrust: Benchmarking trustworthiness in large vision language models for autonomous driving. *arXiv preprint arXiv:2412.15206*, 2024.

- Xu, C., Petiushko, A., Zhao, D., and Li, B. Diffscene: Diffusion-based safety-critical scenario generation for autonomous vehicles. In *Proceedings of the AAAI Conference on Artificial Intelligence*, volume 39, pp. 8797–8805, 2025a.
- Xu, R., Lin, H., Jeon, W., Feng, H., Zou, Y., Sun, L., Gorman, J., Tolstaya, E., Tang, S., White, B., et al. Wod-e2e: Waymo open dataset for end-to-end driving in challenging long-tail scenarios. *arXiv preprint arXiv:2510.26125*, 2025b.
- Zhang, H., Chen, H., Xiao, C., Li, B., Liu, M., Boning, D., and Hsieh, C.-J. Robust deep reinforcement learning against adversarial perturbations on state observations. *Advances in neural information processing systems*, 33: 21024–21037, 2020a.
- Zhang, H., Chen, H., Boning, D., and Hsieh, C.-J. Robust reinforcement learning on state observations with learned optimal adversary. *arXiv preprint arXiv:2101.08452*, 2021.
- Zhang, J., Xu, C., and Li, B. Chatscene: Knowledge-enabled safety-critical scenario generation for autonomous vehicles. In *Proceedings of the IEEE/CVF Conference on Computer Vision and Pattern Recognition*, pp. 15459–15469, 2024.
- Zhang, K., Hu, B., and Basar, T. On the stability and convergence of robust adversarial reinforcement learning: A case study on linear quadratic systems. *Advances in Neural Information Processing Systems*, 33:22056–22068, 2020b.
- Zhang, L., Peng, Z., Li, Q., and Zhou, B. Cat: Closed-loop adversarial training for safe end-to-end driving. In *Conference on Robot Learning*, pp. 2357–2372. PMLR, 2023.
- Zhang, Q., Hu, S., Sun, J., Chen, Q. A., and Mao, Z. M. On adversarial robustness of trajectory prediction for autonomous vehicles. In *Proceedings of the IEEE/CVF Conference on Computer Vision and Pattern Recognition*, pp. 15159–15168, 2022.
- Zhou, W., Cao, Z., Xu, Y., Deng, N., Liu, X., Jiang, K., and Yang, D. Long-tail prediction uncertainty aware trajectory planning for self-driving vehicles. In *2022 IEEE 25th International Conference on Intelligent Transportation Systems (ITSC)*, pp. 1275–1282. IEEE, 2022.

Appendix

The appendix provides rigorous theoretical foundations, supplementary experimental results, and detailed implementation specifications that support the main text. We organize the contents as follows: Section A discusses related work and positions our work in the literature. Section B presents the complete derivations and proofs for the theoretical discussion provided in Section 3.4. We include additional qualitative visualizations and extended quantitative results in Section C to complement the main paper. Finally, Section D details the experimental setups, including the dataset, environment, baselines, implementations, and hyperparameters for reproducibility.

A. Related Work

This section reviews the literature relevant to our approach, with a particular focus on autonomous driving (AD). We position our work at the intersection of three interleaving pathways: RL, long-tailed scenario handling, and adversarial learning.

Reinforcement learning. RL has been widely studied in AD to enable closed-loop decision-making and address the covariate shift inherent in supervised imitation (Kiran et al., 2021; Chen et al., 2024; Karkus et al., 2025). Traditional approaches have largely focused on motion planning and continuous control using vectorized state representations (Isele et al., 2018; Saxena et al., 2020), or vision-based end-to-end driving within high-fidelity simulators (Chen et al., 2019; Toromanoff et al., 2020). These methods typically employ actor-critic algorithms, such as PPO and SAC (Schulman et al., 2017; Haarnoja et al., 2018), to maximize cumulative returns based on handcrafted reward functions. However, reward specification and value estimation in complex driving scenarios remain notoriously difficult (Knox et al., 2023; Chen et al., 2024). To address the difficulties, recent research has shifted toward alignment techniques emerging from large language models (LLMs). This includes learning from human preferences or feedback to recover reward functions from demonstrations (Ouyang et al., 2022). More notably, critic-free methods, such as Direct Preference Optimization (DPO) (Rafailov et al., 2023) and Group Relative Policy Optimization (GRPO) (Guo et al., 2025), are gaining increasing attention. These methods optimize policies directly against preference data or outcomes across rollouts without training unstable value functions, showing promising results in training end-to-end driving autonomy (Jiang et al., 2025; Li et al., 2025a;b).

Long-tailed scenario. Handling long-tailed events remains a longstanding challenge for AD deployment and system trustworthiness (Feng et al., 2021; Liu & Feng, 2024; Xing et al., 2024; Chen et al., 2024; Wang et al., 2025b). To mitigate the scarcity of such data in naturalistic driving and provide high-value testing samples, significant effort has been devoted to safety-critical scenario generation (Ding et al., 2023; Li et al., 2025c). Representative approaches range from rule-based (Tuncali et al., 2018; Zhang et al., 2024; Mei et al., 2024), optimization-based (Wang et al., 2021; Hanselmann et al., 2022; Zhang et al., 2022; 2023; Nie et al., 2025; Mei et al., 2025), to learning-based methods (Ding et al., 2020; Kuutti et al., 2020; Feng et al., 2023; Xu et al., 2025a; Liu et al., 2025). Despite their success in identifying failures, effectively integrating these adversarial generation pipelines into closed-loop training remains an open question: the primary goal of existing methods is often to stress-test the system rather than to improve it. Conversely, a parallel line of research endeavors to enhance the robustness of decision-making in rare events by designing specialized architectures or leveraging the reasoning capabilities of pretrained LLMs/VLMs (Zhou et al., 2022; Tian et al., 2024; Fang et al., 2025; Tian et al., 2025; Xu et al., 2025b; Wang et al., 2025a; Tang et al., 2025). However, adversarial scenario generation and policy improvement are seldom unified in a holistic framework. Consequently, the generalizability of these methods to unseen, open-world long-tailed scenarios remains under-investigated.

Adversarial learning. Adversarial training offers a principled framework for improvement-targeted generation. In the context of robotics and autonomy, adversarial RL has been extensively discussed for control tasks in constrained settings (Pinto et al., 2017; Pan et al., 2019; Tessler et al., 2019; Zhang et al., 2020a;b; Vinitsky et al., 2020; Kamalaruban et al., 2020; Zhang et al., 2021). However, they typically prioritize theoretical analysis within simplified simulation environments with controlled noise, which differs significantly from the complexity of real-world driving. Within the AD domain, adversarial methods have mainly targeted the robustness of perception and detection modules against observation perturbations (Bloor et al., 2019; Tu et al., 2020; 2021; Deng et al., 2021; He et al., 2022; Amirkhani et al., 2023). In contrast, adversarial training for decision-making, particularly regarding long-tailed scenarios, remains underexplored (Ma et al., 2018; Wachi, 2019; Anzalone et al., 2022; Zhang et al., 2023; 2024). Even among the few works addressing this, the generation and training phases are often decoupled. Crucially, they are typically confined to specific policy types or tested against handcrafted adversarial scenarios, which poses significant challenges to their generalizability across diverse and evolving corner cases.

B. Theoretical Analysis

B.1. Convergence Analysis

In this section, we provide a theoretical guarantee for the convergence of the ADV-0 framework. We formulate the interaction between the ego agent π_θ and the adversary \mathcal{G}_ψ as a regularized two-player Zero-Sum Markov Game (ZSMG). Our analysis proceeds in two steps: (1) We first prove that the inner loop optimization via IPL is mathematically equivalent to solving for the soft optimal adversarial distribution subject to a KL-divergence constraint (Lemma B.1). (2) We then elaborate that the alternating soft updates of the defender and the attacker constitute a contraction mapping, guaranteeing convergence to the Nash Equilibrium of the game (Theorem B.3).

B.1.1. PRELIMINARIES: ADV-0 AS A REGULARIZED ZERO-SUM MARKOV GAME

Formally, we define the discounted ZSMG between the ego and the adversary by the tuple $(\mathcal{S}, \mathcal{A}, \mathcal{Y}, \Pi, \Psi, \mathcal{P}, \mathcal{R}, \gamma)$, where:

- The *defender* (ego agent) chooses a policy $\pi_\theta \in \Pi : \mathcal{S} \rightarrow \Delta(\mathcal{A})$ to maximize its expected return.
- The *attacker* (adversary) chooses a generative policy $\mathcal{G}_\psi \in \Psi : \mathcal{X} \rightarrow \Delta(\mathcal{Y})$ to produce adversarial trajectories $Y^{\text{Adv}} \in \mathcal{Y}$, which in turn perturbs the transition dynamics \mathcal{P}_ψ . The attacker’s goal is to minimize the defender’s return.

Let the value function $V^{\pi, \psi}(s)$ represent the expected return of the ego agent under the dynamics induced by adversary. The robust optimization objective (Eq. 1) with the KL-constraint (Eq. 2, to maintain naturalistic priors) is formulated as finding the saddle point of the regularized value function:

$$\max_{\pi} \min_{\mathcal{G}_\psi} \mathcal{J}(\pi, \mathcal{G}_\psi) := \mathbb{E}_X \left[\mathbb{E}_{\tau \sim \pi, \mathcal{P}_\psi} \left[\sum_{t=0}^T \gamma^t \mathcal{R}(s_t, a_t) \right] + \tau \mathbb{D}_{\text{KL}}(\mathcal{G}_\psi(\cdot|X) \parallel \mathcal{G}_{\text{ref}}(\cdot|X)) \right], \quad (9)$$

where \mathcal{P}_ψ denotes the transition dynamics modulated by the adversary’s trajectory $Y \sim \mathcal{G}_\psi(\cdot|X)$, $\tau > 0$ controls the regularization strength. Note that the adversary seeks to minimize the ego’s return subject to staying close to the prior \mathcal{G}_{ref} .

The ultimate goal is to find converged policies (π^*, ψ^*) satisfy the saddle-point inequality condition of a Nash Equilibrium:

$$\mathcal{J}(\pi_\theta, \mathcal{G}_{\psi^*}) \leq \mathcal{J}(\pi^*, \mathcal{G}_{\psi^*}) \leq \mathcal{J}(\pi^*, \mathcal{G}_\psi), \quad \forall \pi_\theta \in \Pi, \mathcal{G}_\psi \in \Psi, \quad (10)$$

implying that neither the defender nor the attacker can unilaterally improve their objective.

B.1.2. INNER LOOP OPTIMALITY VIA IMPLICIT REWARD

We first analyze the inner loop of Algorithm 1, where the adversary’s policy \mathcal{G}_ψ is updated while the ego policy π_θ is held fixed. The core of the inner loop is the IPL objective. We will show that minimizing the IPL loss (Eq. 8) is equivalent to finding the optimal adversarial policy that solves the KL-regularized reward maximization problem.

Consider the inner loop objective defined in Eqs. 2 and 7. For a fixed ego policy π_θ , the adversary seeks to find an optimal policy ψ^* that maximizes the expected risk (minimizes ego return) while remaining close to the reference prior \mathcal{G}_{ref} . Let the reward for the adversary be defined as $r(Y) = -J(\pi_\theta, Y)$. The objective is:

$$\max_{\psi} \mathcal{J}_{\text{inner}}(\mathcal{G}_\psi) = \mathbb{E}_{Y \sim \mathcal{G}_\psi(\cdot|X)} \left[r(Y) - \tau \log \frac{\mathcal{G}_\psi(Y|X)}{\mathcal{G}_{\text{ref}}(Y|X)} \right]. \quad (11)$$

Lemma B.1 (Closed-form optimality of the Gibbs adversary). *For a fixed defender π_θ and a reference adversary \mathcal{G}_{ref} , the global optimum \mathcal{G}^* of the KL-constrained objective in Eq. 11 is given by the Gibbs distribution:*

$$\mathcal{G}^*(Y|X) = \frac{1}{Z(X)} \mathcal{G}_{\text{ref}}(Y|X) \exp \left(-\frac{1}{\tau} J(\pi_\theta, Y) \right), \quad (12)$$

where $Z(X)$ is the partition function. Furthermore, minimizing the IPL loss \mathcal{L}_{IPL} (Eq. 8) is equivalent to performing maximum likelihood estimation on this optimal policy \mathcal{G}^* .

Proof. The proof consists of two parts. First, we derive the closed-form optimal adversarial policy. Let $r(Y) = -J(\pi_\theta, Y)$ be the reward for the adversary. Following the derivation in Rafailov et al. (2023), we express the objective using the Gibbs inequality. The objective can be rewritten as maximizing:

$$\begin{aligned} \mathcal{J}_{\text{inner}}(\mathcal{G}) &= \mathbb{E}_{Y \sim \mathcal{G}} \left[r(Y) - \tau \log \frac{\mathcal{G}(Y|X)}{\mathcal{G}_{\text{ref}}(Y|X)} \right] \\ &= \tau \mathbb{E}_{Y \sim \mathcal{G}} \left[\log \exp\left(\frac{1}{\tau} r(Y)\right) + \log \mathcal{G}_{\text{ref}}(Y|X) - \log \mathcal{G}(Y|X) \right] \\ &= \tau \mathbb{E}_{Y \sim \mathcal{G}} \left[\log \left(\mathcal{G}_{\text{ref}}(Y|X) \exp\left(\frac{r(Y)}{\tau}\right) \right) - \log \mathcal{G}(Y|X) \right]. \end{aligned} \quad (13)$$

Let $Z(X) = \int \mathcal{G}_{\text{ref}}(y|X) \exp(r(y)/\tau) dy$ be the partition function. We can introduce $\log Z(X)$ into the expectation:

$$\begin{aligned} \mathcal{J}_{\text{inner}}(\mathcal{G}) &= \tau \mathbb{E}_{Y \sim \mathcal{G}} \left[\log \left(\frac{1}{Z(X)} \mathcal{G}_{\text{ref}}(Y|X) \exp\left(\frac{r(Y)}{\tau}\right) \right) - \log \mathcal{G}(Y|X) + \log Z(X) \right] \\ &= -\tau \mathbb{D}_{\text{KL}}(\mathcal{G}(\cdot|X) \parallel \mathcal{G}^*(\cdot|X)) + \tau \log Z(X), \end{aligned} \quad (14)$$

where $\mathcal{G}^*(Y|X) = \frac{1}{Z(X)} \mathcal{G}_{\text{ref}}(Y|X) \exp\left(\frac{r(Y)}{\tau}\right)$. Since $\mathbb{D}_{\text{KL}} \geq 0$, the objective is maximized when $\mathcal{G} = \mathcal{G}^*$, proving the first part of the lemma. This first confirms that our energy-based posterior sampling samples exactly from the optimal adversarial distribution. However, explicitly evaluating $Z(X)$ is intractable.

We next show that minimizing the IPL loss \mathcal{L}_{IPL} with respect to ψ is consistent with maximizing the likelihood of the preference data generated by the optimal adversary \mathcal{G}^* , without the need to estimate the partition function. We show the equivalence following Rafailov et al. (2023). We can invert the optimal policy equation to rewrite the reward as:

$$r(Y) = \tau \log \frac{\mathcal{G}^*(Y|X)}{\mathcal{G}_{\text{ref}}(Y|X)} + \tau \log Z(X). \quad (15)$$

Under the Bradley-Terry preference model, the probability that trajectory Y_w is preferred over Y_l (i.e., Y_w induces lower ego return) is given by $P(Y_w \succ Y_l) = \sigma(r(Y_w) - r(Y_l))$. Substituting the reparameterized reward into this model:

$$\begin{aligned} P(Y_w \succ Y_l) &= \sigma \left(\left(\tau \log \frac{\mathcal{G}^*(Y_w|X)}{\mathcal{G}_{\text{ref}}(Y_w|X)} + \tau \log Z \right) - \left(\tau \log \frac{\mathcal{G}^*(Y_l|X)}{\mathcal{G}_{\text{ref}}(Y_l|X)} + \tau \log Z \right) \right) \\ &= \sigma \left(\tau \log \frac{\mathcal{G}^*(Y_w|X)}{\mathcal{G}_{\text{ref}}(Y_w|X)} - \tau \log \frac{\mathcal{G}^*(Y_l|X)}{\mathcal{G}_{\text{ref}}(Y_l|X)} \right). \end{aligned} \quad (16)$$

The partition function $Z(X)$ cancels out. The IPL loss (Eq. 8) is exactly the negative log-likelihood of this probability with the parameterized policy \mathcal{G}_ψ approximating \mathcal{G}^* . Thus, minimizing \mathcal{L}_{IPL} is equivalent to fitting the optimal adversarial policy \mathcal{G}^* consistent with the observed preferences. This proves that the inner loop of ADV-0 effectively solves the constrained optimization problem in Eq. 2. \square

B.1.3. GLOBAL CONVERGENCE TO NASH EQUILIBRIUM

Having established in Lemma B.1 that the inner loop via IPL effectively recovers the optimal adversarial distribution \mathcal{G}_{ψ^*} , we now analyze the convergence of the global alternating optimization. We show that the entire ADV-0 framework can be viewed as optimizing a specific robust Bellman Operator, which guarantees convergence to a unique Nash Equilibrium.

Before beginning the formal derivation, we first establish the following Lemma:

Lemma B.2 (Non-expansiveness of Soft-Min). *Let $f_\tau(X) \triangleq -\tau \log \mathbb{E}_Y [\exp(-X(Y)/\tau)]$ be the Soft-Min operator over a random variable Y with temperature $\tau > 0$. For any two bounded functions X_1, X_2 , the following inequality holds:*

$$|f_\tau(X_1) - f_\tau(X_2)| \leq \max_Y |X_1(Y) - X_2(Y)|. \quad (17)$$

Proof. Let $\Delta = \max_Y |X_1(Y) - X_2(Y)|$. By definition, for all Y , the difference is bounded by:

$$X_2(Y) - \Delta \leq X_1(Y) \leq X_2(Y) + \Delta. \quad (18)$$

Multiplying by $-1/\tau$ and exponentiating yields:

$$\exp\left(\frac{-X_2(Y) - \Delta}{\tau}\right) \leq \exp\left(\frac{-X_1(Y)}{\tau}\right) \leq \exp\left(\frac{-X_2(Y) + \Delta}{\tau}\right). \quad (19)$$

Taking the expectation \mathbb{E}_Y preserves the inequality. We can factor out the constant terms $\exp(\pm\Delta/\tau)$:

$$e^{-\Delta/\tau} \mathbb{E}_Y[e^{-X_2(Y)/\tau}] \leq \mathbb{E}_Y[e^{-X_1(Y)/\tau}] \leq e^{\Delta/\tau} \mathbb{E}_Y[e^{-X_2(Y)/\tau}]. \quad (20)$$

Next, we apply the strictly decreasing function $-\tau \log(\cdot)$ to all sides. We have:

$$-\tau \log\left(e^{\Delta/\tau} \mathbb{E}[e^{-X_2/\tau}]\right) \leq -\tau \log \mathbb{E}[e^{-X_1/\tau}] \leq -\tau \log\left(e^{-\Delta/\tau} \mathbb{E}[e^{-X_2/\tau}]\right). \quad (21)$$

Using the definition of f_τ and expanding the terms:

$$f_\tau(X_2) - \Delta \leq f_\tau(X_1) \leq f_\tau(X_2) + \Delta. \quad (22)$$

Subtracting $f_\tau(X_2)$ from all sides, we obtain:

$$-\Delta \leq f_\tau(X_1) - f_\tau(X_2) \leq \Delta. \quad (23)$$

This is equivalent to $|f_\tau(X_1) - f_\tau(X_2)| \leq \Delta$. \square

Theorem B.3 (Contraction and convergence to Nash Equilibrium). *Let \mathcal{V} be the space of bounded value functions equipped with the L_∞ -norm. The Soft-Robust Bellman Operator $\mathcal{T}_{rob} : \mathcal{V} \rightarrow \mathcal{V}$, defined as:*

$$(\mathcal{T}_{rob}V)(s) \triangleq \max_{a \in \mathcal{A}} \min_{\mathcal{G}_\psi \in \Psi} \left(\mathcal{R}(s, a) + \gamma \mathbb{E}_{\substack{Y \sim \mathcal{G}_\psi \\ s' \sim \mathcal{P}(\cdot|s, a, Y)}} [V(s')] + \tau \mathbb{D}_{KL}(\mathcal{G}_\psi || \mathcal{G}_{ref}) \right), \quad (24)$$

is a γ -contraction mapping. Specifically, for any two value functions $V, U \in \mathcal{V}$, the following inequality holds:

$$\|\mathcal{T}_{rob}V - \mathcal{T}_{rob}U\|_\infty \leq \gamma \|V - U\|_\infty. \quad (25)$$

Consequently, the iterative updates in ADV-0 converge to a unique fixed point V^* . This fixed point corresponds to the value of the unique Nash Equilibrium $(\pi^*, \mathcal{G}_{\psi^*})$ of the regularized zero-sum game, satisfying the saddle-point inequality:

$$\mathcal{J}_\tau(\pi, \mathcal{G}_{\psi^*}) \leq \mathcal{J}_\tau(\pi^*, \mathcal{G}_{\psi^*}) \leq \mathcal{J}_\tau(\pi^*, \mathcal{G}_\psi), \quad \forall \pi \in \Pi, \forall \mathcal{G}_\psi \in \Psi, \quad (26)$$

where $\mathcal{J}_\tau(\pi, \mathcal{G}_\psi) \triangleq \mathbb{E}_{\pi, \mathcal{G}_\psi} [\sum \gamma^t \mathcal{R}(s_t, a_t)] + \tau \mathbb{E}_\pi [\sum \gamma^t \mathbb{D}_{KL}(\mathcal{G}_\psi || \mathcal{G}_{ref})]$ is the regularized cumulative objective.

Proof. First, we define the soft-robust Bellman operator \mathcal{T}_{rob} acting on the value function $V \in \mathbb{R}^{|\mathcal{S}|}$:

$$(\mathcal{T}_{rob}V)(s) = \max_{a \in \mathcal{A}} \min_{\mathcal{G}_\psi} \mathbb{E}_{Y \sim \mathcal{G}_\psi} \left[\mathcal{R}(s, a) + \gamma \mathbb{E}_{s' \sim \mathcal{P}(s, a, Y)} [V(s')] + \tau \log \frac{\mathcal{G}_\psi(Y|X)}{\mathcal{G}_{ref}(Y|X)} \right]. \quad (27)$$

This operator represents one step of optimal decision-making by the ego agent against a worst-case adversary that is regularized by the KL-divergence. Note that the inner minimization in \mathcal{T}_{rob} corresponds exactly to the dual of the maximization problem in Lemma B.1 (due to the zero-sum sign flip).

Next, let $V_1, V_2 \in \mathbb{R}^{|\mathcal{S}|}$ be two arbitrary bounded value functions. We aim to show $\|\mathcal{T}_{rob}V_1 - \mathcal{T}_{rob}V_2\|_\infty \leq \gamma \|V_1 - V_2\|_\infty$. We simplify the inner minimization problem. Let $\mathcal{Q}_V(s, a, Y) = \mathcal{R}(s, a) + \gamma \mathbb{E}_{s' \sim \mathcal{P}(s, a, Y)} [V(s')]$. Using the closed-form solution derived in Lemma B.1, the inner minimization over \mathcal{G}_ψ is equivalent to a `LogSumExp` (Soft-Min) function. We define the smoothed value $\Omega_V(s, a)$ as:

$$\Omega_V(s, a) \triangleq \min_{\mathcal{G}_\psi} \mathbb{E}_{Y \sim \mathcal{G}_\psi} \left[\mathcal{Q}_V(s, a, Y) + \tau \log \frac{\mathcal{G}_\psi(Y|X)}{\mathcal{G}_{ref}(Y|X)} \right] = -\tau \log \mathbb{E}_{Y \sim \mathcal{G}_{ref}} \left[\exp\left(-\frac{\mathcal{Q}_V(s, a, Y)}{\tau}\right) \right]. \quad (28)$$

Thus, the operator simplifies to $(\mathcal{T}_{\text{rob}}V)(s) = \max_a \Omega_V(s, a)$. Consider the difference for any state s :

$$\begin{aligned} |(\mathcal{T}_{\text{rob}}V_1)(s) - (\mathcal{T}_{\text{rob}}V_2)(s)| &= \left| \max_a \Omega_{V_1}(s, a) - \max_a \Omega_{V_2}(s, a) \right| \\ &\leq \max_a |\Omega_{V_1}(s, a) - \Omega_{V_2}(s, a)|. \end{aligned} \quad (29)$$

where Eq. 29 follows from the non-expansiveness of the max operator (i.e., $|\max f - \max g| \leq \max |f - g|$). Next, we apply Lemma B.2 to the soft-min term Ω_V . By identifying $X(Y)$ with $Q_V(s, a, Y)$, we obtain:

$$\begin{aligned} |\Omega_{V_1}(s, a) - \Omega_{V_2}(s, a)| &= \left| -\tau \log \frac{\mathbb{E}_Y[\exp(-Q_{V_1}(s, a, Y)/\tau)]}{\mathbb{E}_Y[\exp(-Q_{V_2}(s, a, Y)/\tau)]} \right| \\ &\leq \max_Y \left| -\tau \left(-\frac{Q_{V_1}(s, a, Y)}{\tau} + \frac{Q_{V_2}(s, a, Y)}{\tau} \right) \right| \\ &= \max_Y |Q_{V_1}(s, a, Y) - Q_{V_2}(s, a, Y)|. \end{aligned} \quad (30)$$

Substituting the definition of Q_V and expanding the expectation:

$$\begin{aligned} &= \max_Y \left| \gamma \mathbb{E}_{s' \sim \mathcal{P}(\cdot|s, a, Y)} [V_1(s') - V_2(s')] \right| \\ &\leq \gamma \max_Y \mathbb{E}_{s'} [|V_1(s') - V_2(s')|] \quad (\text{Jensen's inequality}) \\ &\leq \gamma \|V_1 - V_2\|_{\infty}. \quad (\text{Definition of } L_{\infty}\text{-norm}) \end{aligned} \quad (31)$$

The last two steps utilize the convexity of the absolute value function and bound the local error by the global supremum norm. Since $\gamma \in (0, 1)$, \mathcal{T}_{rob} is a γ -contraction mapping. By Banach's Fixed Point Theorem, there exists a unique value V^* such that $\mathcal{T}_{\text{rob}}V^* = V^*$.

Finally, we connect this to the alternating updates in Algorithm 1. The algorithm performs generalized policy iteration. The inner loop (IPL) solves for the optimal soft adversary via gradient descent on the KL-regularized objective, effectively evaluating $\Omega_{V^*}(s, a)$. The outer loop performs standard RL optimization on the induced robust value function. Tessler et al. (2019) (Theorem 3) and Scherrer (2014) demonstrate that soft policy iteration converges to the optimal value if the policy improvement step is a contraction. Since \mathcal{T}_{rob} is a contraction, the sequence of policies (π_k, ψ_k) generated by ADV-0 converges to the Nash Equilibrium (π^*, ψ^*) where π^* is optimal against the worst-case regularized adversary ψ^* . \square

B.2. Generalization Bound and Safety Guarantees

In this section, we provide a theoretical justification of ADV-0 in its generalizability and safety guarantees. We aim to answer a fundamental question: *Does optimizing the policy against a generated adversarial distribution guarantee performance and safety in the real-world long-tail distribution?* Different from the previous section, we now model the interaction between the ego policy π_{θ} and the adversarial environment as a problem of policy optimization under dynamical uncertainty. Our goal is to show that optimizing the policy under the adversarial dynamics \mathcal{P}_{ψ} (subject to the KL-constraint in the inner loop) maximizes a certified lower bound on the performance in the target real-world long-tail distribution $\mathcal{P}_{\text{real}}$, leading to a **generalization bound** (Theorem B.6) and a **safety guarantee** (Theorem B.8). Our analysis builds upon the *Simulation Lemma* from Luo et al. (2018) and trust-region bounds from Achiam et al. (2017).

Preliminaries. Simply let $M = (\mathcal{S}, \mathcal{A}, \mathcal{R}, \gamma)$ be the shared components of the MDP. We consider two transition dynamics:

- $\mathcal{P}_{\text{real}}(s'|s, a)$: The true, unknown long-tail dynamics of the real world.
- $\mathcal{P}_{\psi}(s'|s, a)$: The adversarial dynamics induced by the generator $\mathcal{G}_{\psi}(\cdot|X)$.

In our context, the state transition is deterministic given the background traffic trajectories. Let Y denote the joint trajectory of background agents. The transition function can be written as $s' = f(s, a, Y)$. Thus, the stochasticity in dynamics comes entirely from the distribution of Y . Let $V^{\pi, \mathcal{P}}(s) = \mathbb{E}_{\tau \sim \pi, \mathcal{P}} [\sum_{t=0}^{\infty} \gamma^t \mathcal{R}(s_t, a_t) | s_0 = s]$ be the value function. The expected return is $J(\pi, \mathcal{P}) = \mathbb{E}_{s_0 \sim \rho_0} [V^{\pi, \mathcal{P}}(s_0)]$. Similarly, let $J_C(\pi, \mathcal{P})$ denote the expected cumulative safety cost, where $C(s, a) \in [0, C_{\text{max}}]$ is a safety cost function (e.g., collision indicator). We assume the reward is bounded by R_{max} , implying the value function is bounded by $V_{\text{max}} = \frac{R_{\text{max}}}{1-\gamma}$.

B.2.1. DISCREPANCY UNDER SHIFTED DYNAMICS

To analyze performance generalization, we first quantify the discrepancy in expected return resulting from the shift from real dynamics to adversarial dynamics. We invoke the Simulation Lemma (Achiam et al., 2017) and adapt here to quantify the gap between the adversarial training environment and the real world.

Lemma B.4 (Value difference under dynamics shift). *For any fixed policy π and two transition dynamics \mathcal{P} and \mathcal{P}' , the difference in expected return is:*

$$J(\pi, \mathcal{P}) - J(\pi, \mathcal{P}') = \gamma \sum_{t=0}^{\infty} \gamma^t \mathbb{E}_{s_t \sim \pi, \mathcal{P}, a_t \sim \pi} \left[\mathbb{E}_{s' \sim \mathcal{P}(\cdot | s_t, a_t)} [V^{\pi, \mathcal{P}'}(s')] - \mathbb{E}_{s' \sim \mathcal{P}'(\cdot | s_t, a_t)} [V^{\pi, \mathcal{P}'}(s')] \right]. \quad (32)$$

Proof. We use the telescoping sum technique, following Lemma 4.3 in Luo et al. (2018). Let $V^{\mathcal{P}'}$ denote $V^{\pi, \mathcal{P}'}$ for brevity. Remind that $-V^{\mathcal{P}'}(s_0) = \sum_{t=0}^{\infty} \gamma^t (\gamma V^{\mathcal{P}'}(s_{t+1}) - V^{\mathcal{P}'}(s_t)) - \lim_{T \rightarrow \infty} \gamma^T V^{\mathcal{P}'}(s_T)$, we expand the difference as follows:

$$\begin{aligned} J(\pi, \mathcal{P}) - J(\pi, \mathcal{P}') &= \mathbb{E}_{s_0} [V^{\pi, \mathcal{P}}(s_0) - V^{\pi, \mathcal{P}'}(s_0)] \\ &= \mathbb{E}_{\tau \sim \pi, \mathcal{P}} \left[\sum_{t=0}^{\infty} \gamma^t \mathcal{R}(s_t, a_t) \right] - \mathbb{E}_{s_0} [V^{\mathcal{P}'}(s_0)] \\ &= \mathbb{E}_{\tau \sim \pi, \mathcal{P}} \left[\sum_{t=0}^{\infty} \gamma^t \mathcal{R}(s_t, a_t) + \sum_{t=0}^{\infty} \gamma^t (\gamma V^{\mathcal{P}'}(s_{t+1}) - V^{\mathcal{P}'}(s_t)) - \lim_{T \rightarrow \infty} \gamma^T V^{\mathcal{P}'}(s_T) \right] \\ &= \mathbb{E}_{\tau \sim \pi, \mathcal{P}} \left[\sum_{t=0}^{\infty} \gamma^t \left(\mathcal{R}(s_t, a_t) + \gamma V^{\mathcal{P}'}(s_{t+1}) - V^{\mathcal{P}'}(s_t) \right) \right]. \end{aligned} \quad (33)$$

Recall the Bellman equation for $V^{\mathcal{P}'}$ is $V^{\mathcal{P}'}(s) = \mathbb{E}_{a \sim \pi} [\mathcal{R}(s, a) + \gamma \mathbb{E}_{s' \sim \mathcal{P}'} [V^{\mathcal{P}'}(s')]]$. Substituting $\mathcal{R}(s_t, a_t) = V^{\mathcal{P}'}(s_t) - \gamma \mathbb{E}_{s' \sim \mathcal{P}'(\cdot | s_t, a_t)} [V^{\mathcal{P}'}(s')]$ into the summation, the term $V^{\mathcal{P}'}(s_t)$ cancels out:

$$\begin{aligned} J(\pi, \mathcal{P}) - J(\pi, \mathcal{P}') &= \mathbb{E}_{\tau \sim \pi, \mathcal{P}} \left[\sum_{t=0}^{\infty} \gamma^t \left(V^{\mathcal{P}'}(s_t) - \gamma \mathbb{E}_{s' \sim \mathcal{P}'} [V^{\mathcal{P}'}(s')] + \gamma V^{\mathcal{P}'}(s_{t+1}) - V^{\mathcal{P}'}(\cdot | s_t, a_t)(s_t) \right) \right] \\ &= \mathbb{E}_{\tau \sim \pi, \mathcal{P}} \left[\sum_{t=0}^{\infty} \gamma^t \left(\gamma V^{\mathcal{P}'}(s_{t+1}) - \gamma \mathbb{E}_{s' \sim \mathcal{P}'(\cdot | s_t, a_t)} [V^{\mathcal{P}'}(s')] \right) \right] \\ &= \sum_{t=0}^{\infty} \gamma^{t+1} \mathbb{E}_{\substack{s_t \sim \pi, \mathcal{P} \\ a_t \sim \pi}} \left[\mathbb{E}_{s_{t+1} \sim \mathcal{P}(\cdot | s_t, a_t)} [V^{\mathcal{P}'}(s_{t+1})] - \mathbb{E}_{s' \sim \mathcal{P}'(\cdot | s_t, a_t)} [V^{\mathcal{P}'}(s')] \right]. \end{aligned} \quad (34)$$

Adjusting the index of summation yields the lemma statement. \square

Lemma B.4 suggests that the performance differences depend on the differences of transition dynamics, but in ADV-0 we optimize \mathcal{G}_ψ , not \mathcal{P}_ψ directly. To fill this gap, we establish the connection between the dynamics divergence and the generator divergence in the following lemma.

Lemma B.5 (Divergence bound of the generator). *Let \mathcal{P} and \mathcal{P}' be the transition dynamics induced by the trajectory generators \mathcal{G} and \mathcal{G}' , respectively. Specifically, the next state is obtained by a deterministic simulator $s' = F(s, a, Y)$, where Y is the adversarial trajectory sampled from the generator. For any value function $V^{\pi, \mathcal{P}'}$ bounded by $V_{\max} = \frac{R_{\max}}{1-\gamma}$, the difference in expected next-state value is bounded by the Total Variation (TV) divergence of the generators:*

$$\left| \mathbb{E}_{s' \sim \mathcal{P}(\cdot | s, a)} [V^{\pi, \mathcal{P}'}(s')] - \mathbb{E}_{s' \sim \mathcal{P}'(\cdot | s, a)} [V^{\pi, \mathcal{P}'}(s')] \right| \leq 2V_{\max} \cdot \mathbb{E}_X [D_{TV}(\mathcal{G}(\cdot | X) \| \mathcal{G}'(\cdot | X))]. \quad (35)$$

Proof. We start by explicitly writing the expectation over the next state s' as an expectation over the generated trajectories Y , i.e., $\mathbb{E}_{s' \sim \mathcal{P}} [V(s')] = \int \mathcal{G}(Y|X) \cdot V(F_{\text{phy}}(s, a, Y)) dY$. Let $p(Y|X)$ and $q(Y|X)$ denote the probability density functions of the generators \mathcal{G} and \mathcal{G}' conditioned on context X . Since $s' = F(s, a, Y)$, the expectation can be rewritten via the change

of variables:

$$\begin{aligned}\Delta_V &= \left| \mathbb{E}_{s' \sim \mathcal{P}}[V^{\pi, \mathcal{P}'}(s')] - \mathbb{E}_{s' \sim \mathcal{P}'}[V^{\pi, \mathcal{P}'}(s')] \right| \\ &= \left| \int p(Y|X) V^{\pi, \mathcal{P}'}(F(s, a, Y)) dY - \int q(Y|X) V^{\pi, \mathcal{P}'}(F(s, a, Y)) dY \right|,\end{aligned}\quad (36)$$

$$= \left| \int (p(Y|X) - q(Y|X)) \cdot V^{\pi, \mathcal{P}'}(F(s, a, Y)) dY \right|.\quad (37)$$

Next, we apply the integral form of Hölder's inequality ($|\int f(x)g(x)dx| \leq \int |f(x)||g(x)|dx \leq \|f\|_1 \|g\|_\infty$). Here, we treat the probability difference as the measure and the value function as the bounded term:

$$\begin{aligned}\Delta_V &\leq \int |p(Y|X) - q(Y|X)| \cdot |V^{\pi, \mathcal{P}'}(F(s, a, Y))| dY \\ &\leq \underbrace{\left(\int |p(Y|X) - q(Y|X)| dY \right)}_{\|p-q\|_1} \cdot \underbrace{\sup_Y |V^{\pi, \mathcal{P}'}(F(s, a, Y))|}_{\|V\|_\infty}.\end{aligned}\quad (38)$$

We then use two key properties: 1. The L_1 norm of the difference between two probability distributions is twice the Total Variation distance: $\|p - q\|_1 = 2D_{\text{TV}}(p, q)$. 2. The value function is bounded by the maximum possible cumulative return: $\|V\|_\infty \leq V_{\text{max}} = R_{\text{max}}/1 - \gamma$. Substituting these back into the inequality, we obtain:

$$\Delta_V \leq 2D_{\text{TV}}(\mathcal{G}(\cdot|X) \|\mathcal{G}'(\cdot|X)) \cdot V_{\text{max}}.\quad (39)$$

Taking the expectation over the context distribution X completes the proof. This lemma serves as a crucial bridge in our analysis: it formally translates the divergence in the high-level trajectory generator space (which we explicitly optimize and constrain via IPL) into the divergence in the low-level state transition space, thereby allowing us to bound the error. \square

B.2.2. ADVERSARIAL GENERALIZATION BOUND

Finally, we present the main theorem. We show that the policy π_θ trained by ADV-0 maximizes a lower bound on the performance in real-world distribution. IPL loop enforces a KL-constraint between the adversary \mathcal{G}_ψ and the prior \mathcal{G}_{ref} .

Theorem B.6 (Lower bound of adversarial generalization). *Let π_θ be the policy trained under adversarial dynamics \mathcal{P}_ψ . The expected return of π_θ under the real-world dynamics $\mathcal{P}_{\text{real}}$ is lower-bounded by:*

$$J(\pi_\theta, \mathcal{P}_{\text{real}}) \geq J(\pi_\theta, \mathcal{P}_\psi) - \frac{\gamma V_{\text{max}} \sqrt{2}}{1 - \gamma} \sqrt{\mathbb{E}_X [D_{\text{KL}}(\mathcal{G}_\psi(\cdot|X) \|\mathcal{G}_{\text{ref}}(\cdot|X))]}.\quad (40)$$

Proof. The proof utilizes the established lemmas above. We first invoke Lemma B.4 with $\mathcal{P} = \mathcal{P}_{\text{real}}$ and $\mathcal{P}' = \mathcal{P}_\psi$:

$$|J(\pi, \mathcal{P}_{\text{real}}) - J(\pi, \mathcal{P}_\psi)| \leq \gamma \sum_{t=0}^{\infty} \gamma^t \left| \mathbb{E}_{s_t, a_t} \left[\mathbb{E}_{s' \sim \mathcal{P}_{\text{real}}} [V^{\pi, \mathcal{P}_\psi}(s')] - \mathbb{E}_{s' \sim \mathcal{P}_\psi} [V^{\pi, \mathcal{P}_\psi}(s')] \right] \right|.\quad (41)$$

Given that the reference generator \mathcal{G}_{ref} is trained on large-scale naturalistic driving logs (WOMD), we assume that the dynamics induced by \mathcal{G}_{ref} serve as a high-fidelity approximation of the real-world dynamics $\mathcal{P}_{\text{real}}$. Consequently, by applying Lemma B.5 with $\mathcal{G}' = \mathcal{G}_{\text{ref}}$, we bound the inner term:

$$\left| \mathbb{E}_{\mathcal{P}_{\text{real}}} [V^{\pi, \mathcal{P}_\psi}] - \mathbb{E}_{\mathcal{P}_\psi} [V^{\pi, \mathcal{P}_\psi}] \right| \leq 2V_{\text{max}} \mathbb{E}_X [D_{\text{TV}}(\mathcal{G}_{\text{ref}}(\cdot|X) \|\mathcal{G}_\psi(\cdot|X))].\quad (42)$$

Substituting this bound back into the summation and using the geometric series sum $\sum_{t=0}^{\infty} \gamma^t = \frac{1}{1-\gamma}$:

$$J(\pi, \mathcal{P}_{\text{real}}) \geq J(\pi, \mathcal{P}_\psi) - \frac{2\gamma V_{\text{max}}}{1 - \gamma} \mathbb{E}_X [D_{\text{TV}}(\mathcal{G}_{\text{ref}} \|\mathcal{G}_\psi)].\quad (43)$$

Finally, we utilize the symmetry of the Total Variation distance, i.e., $D_{\text{TV}}(P\|Q) = D_{\text{TV}}(Q\|P)$, to equate $D_{\text{TV}}(\mathcal{G}_{\text{ref}}\|\mathcal{G}_{\psi}) = D_{\text{TV}}(\mathcal{G}_{\psi}\|\mathcal{G}_{\text{ref}})$. We then apply Pinsker’s Inequality $D_{\text{TV}}(P\|Q) \leq \sqrt{\frac{1}{2}D_{\text{KL}}(P\|Q)}$ alongside Jensen’s inequality $\mathbb{E}[\sqrt{Z}] \leq \sqrt{\mathbb{E}[Z]}$:

$$\mathbb{E}_X[D_{\text{TV}}(\mathcal{G}_{\text{ref}}\|\mathcal{G}_{\psi})] = \mathbb{E}_X[D_{\text{TV}}(\mathcal{G}_{\psi}\|\mathcal{G}_{\text{ref}})] \leq \sqrt{\frac{1}{2}\mathbb{E}_X[D_{\text{KL}}(\mathcal{G}_{\psi}\|\mathcal{G}_{\text{ref}})]}. \quad (44)$$

Combining these yields the theorem. □

Remark B.7. Theorem B.6 theoretically justifies the objective of ADV-0. The outer loop maximizes the first term $J(\pi_{\theta}, \mathcal{P}_{\psi})$ (robustness), while the IPL inner loop minimizes the second term (generalization gap) by constraining the KL divergence. Thus, our method effectively maximizes a certified lower bound on the real-world performance. Crucially, $\mathcal{P}_{\text{real}}$ here represents any target distribution within the δ -trust region of the prior, specifically including the real-world long-tail scenarios. Since the adversary \mathcal{P}_{ψ} is optimized to be the worst-case minimizer within this region, the theorem guarantees that the policy’s performance on the synthetic adversarial cases serves as a robust lower bound for its performance on unseen real-world critical events.

B.2.3. SAFETY GUARANTEE IN THE LONG TAIL

Finally, we derive the formal safety guarantee. We denote $J_C(\pi, \mathcal{P})$ the expected cumulative cost (e.g., collision risk).

Theorem B.8 (Worst-case safety certificate). *Let C_{max} be the maximum instantaneous cost (upper bound of the per-step cost). If the policy π_{θ} satisfies the safety constraint $J_C(\pi_{\theta}, \mathcal{P}_{\psi}) \leq \delta$ under the adversarial dynamics, then the safety violation in the real environment is bounded by:*

$$J_C(\pi_{\theta}, \mathcal{P}_{\text{real}}) \leq \delta + \frac{\gamma C_{\text{max}} \sqrt{2}}{(1-\gamma)^2} \sqrt{\mathbb{E}_X[D_{\text{KL}}(\mathcal{G}_{\psi}(\cdot|X)\|\mathcal{G}_{\text{ref}}(\cdot|X))]} \quad (45)$$

Proof. The proof follows similar logic as Lemma B.4 and Theorem B.6. We explicitly extend Corollary 2 of Achiam et al. (2017) (which bounds cost performance under policy shifts) to the setting of adversarial dynamics shifts. Formally, we apply Lemma B.4 to the cost value function $V_C^{\pi, \mathcal{P}}$.

$$\begin{aligned} J_C(\pi, \mathcal{P}_{\text{real}}) &\leq J_C(\pi, \mathcal{P}_{\psi}) + |J_C(\pi, \mathcal{P}_{\text{real}}) - J_C(\pi, \mathcal{P}_{\psi})| \\ &\leq \delta + \frac{\gamma}{1-\gamma} \sum_{t=0}^{\infty} (1-\gamma)\gamma^t |\mathbb{E}_{s,a}[V_C] - \mathbb{E}_{\mathcal{P}_{\psi}}[V_C]|. \end{aligned} \quad (46)$$

Using Lemma B.5 with $\|V_C\|_{\infty} \leq \frac{C_{\text{max}}}{1-\gamma}$:

$$J_C(\pi, \mathcal{P}_{\text{real}}) \leq \delta + \frac{\gamma}{(1-\gamma)} \cdot \frac{2C_{\text{max}}}{1-\gamma} \mathbb{E}_X[D_{\text{TV}}(\mathcal{G}_{\text{ref}}\|\mathcal{G}_{\psi})]. \quad (47)$$

Applying Pinsker’s inequality again completes the proof. □

Remark B.9. Theorem B.8 provides a formal safety certificate. It implies that if ADV-0 successfully trains the agent to be safe ($\leq \delta$) against a worst-case adversary \mathcal{P}_{ψ} (which is explicitly designed to maximize risk in Eq. 1) that is constrained to be physically plausible, the agent is guaranteed to be safe in the naturalistic environment up to a margin controlled by the KL divergence in IPL.

B.3. Discussion on Theoretical Assumptions and Practical Implementation

The theoretical results established in Sections B.1 and B.2 provide the formal motivation for ADV-0, which characterizes the ideal behavior of the ZSMG. In practice, our implementation involves necessary approximations to ensure computational tractability. Here, we discuss the validity of these principled approximations and how they connect to the theoretical results. In general, ADV-0 solves the theoretical ZSMG via efficient approximations. The theoretical analysis identifies *what* to optimize (min-max objective with KL regularization) and *why* (maximizing a lower bound on real-world performance), while the practical implementation provides a tractable *how* (IPL with finite sampling).

Finite sample approximation of the Gibbs adversary. Lemma B.1 derives the optimal adversarial distribution as a Gibbs distribution $\mathcal{G}^*(Y|X) \propto \mathcal{G}_{\text{ref}}(Y|X) \exp(-J(\pi_\theta, Y)/\tau)$. In the theoretical analysis, the expectation is taken over the entire continuous trajectory space \mathcal{Y} . In our implementation (Eq. 6), we approximate the intractable partition function $Z(X)$ and the expectation $\mathbb{E}_{Y \sim \mathcal{G}_\psi}$ using importance sampling with a finite set of K candidates $\{Y_k\}_{k=1}^K$ sampled from the proposal distribution \mathcal{G}_ψ . While finite sampling introduces variance, the temperature-scaled softmax sampling serves as a Monte Carlo approximation of the theoretical Boltzmann distribution. As the sample size K increases, the empirical distribution converges to the theoretical optimal adversary. Since the backbone generator is designed to capture the multi-modal nature of the traffic prior. A moderate K (e.g., $K = 32$) effectively covers the high-probability modes of the prior support, ensuring that the empirical distribution converges towards the theoretical Gibbs distribution.

Proxy reward and bias. The inner loop optimization relies on the proxy reward estimator \hat{J} rather than the exact rollout return J . This could introduce bias in the gradient direction. However, we note that the effectiveness of IPL depends primarily on the *ranking* accuracy rather than the precision of *absolute value*. Under the Bradley-Terry model, the probability of preference depends on the value difference: $P(Y_w \succ Y_l) = \sigma(\hat{J}(Y_l) - \hat{J}(Y_w))$. The convergence requires that the proxy estimator preserves the relative ordinality of the true objective, i.e., $J(Y_a) < J(Y_b) \implies \mathbb{E}[\hat{J}(Y_a)] < \mathbb{E}[\hat{J}(Y_b)]$. This means that as long as the proxy estimator preserves the relative ordering of safety-critical events (e.g., correctly identifying that a collision is worse than a near-miss), the gradient direction for ψ remains consistent with the theoretical objective.

Trust region assumption in generalization. Theorem B.6 and B.8 rely on the assumption that the real-world dynamics $\mathcal{P}_{\text{real}}$ lie within a trust region support of the traffic prior \mathcal{G}_{ref} . While this is a strong assumption, it is a necessary condition for data-driven simulation approaches. This formalizes the requirement that the long tail consists of rare but plausible events, rather than out-of-domain anomalies. In the context of ADV-0, this assumption is a constraint enforced by the traffic prior. The term $\mathbb{E}[D_{\text{KL}}(\mathcal{G}_\psi || \mathcal{G}_{\text{ref}})]$ in the generalization bound directly corresponds to the regularization term in the IPL loss (Eq. 8). By minimizing this KL-divergence during training, ADV-0 explicitly optimizes the policy to maximize the lower bound on performance across the entire δ -neighborhood of the naturalistic prior. This ensures that as long as the real-world long-tail events fall within the physical plausibility modeled by the pretrained generator, the safety guarantees hold.

C. Supplementary Tables and Figures

Table 6. Detailed results of safety-critical scenario generation using ADV-0.

ADV-0 Variation	Replay		IDM		RL Agent	
	CR \uparrow	Reward \downarrow	CR \uparrow	Reward \downarrow	CR \uparrow	Reward \downarrow
Pretrained (logit-based sampling)	31.72% \pm 1.06%	43.31 \pm 1.10	18.84% \pm 1.48%	50.66 \pm 2.22	12.49% \pm 1.06%	52.12 \pm 2.03
Pretrained (energy-based sampling)	85.09% \pm 1.13%	1.89 \pm 0.20	40.14% \pm 1.06%	45.72 \pm 0.47	36.30% \pm 0.77%	41.99 \pm 0.33
GRPO Finetuned	92.61 \pm 0.62%	0.87 \pm 0.06	46.34 \pm 0.73%	39.60 \pm 0.13	41.95 \pm 0.47%	38.45 \pm 0.42
PPO Finetuned	90.93 \pm 0.69%	1.01 \pm 0.07	45.09 \pm 0.63%	40.69 \pm 0.22	39.12 \pm 0.38%	39.63 \pm 0.43
SAC Finetuned	91.88 \pm 0.86%	1.03 \pm 0.08	46.09 \pm 0.19%	39.62 \pm 0.24	41.09 \pm 0.59%	39.17 \pm 0.48
TD3 Finetuned	89.54 \pm 0.62%	1.07 \pm 0.06	46.08 \pm 0.42%	39.38 \pm 0.11	40.35 \pm 0.84%	39.68 \pm 0.72
PPO-Lag Finetuned	90.08 \pm 0.42%	1.01 \pm 0.07	45.74 \pm 0.22%	40.50 \pm 0.09	41.30 \pm 0.50%	38.77 \pm 0.39
SAC-Lag Finetuned	91.54 \pm 0.24%	0.95 \pm 0.04	45.61 \pm 0.31%	40.38 \pm 0.06	40.28 \pm 0.73%	39.07 \pm 0.37
Avg.	91.10 \pm 0.57%	0.99 \pm 0.06	45.83 \pm 0.42%	40.03 \pm 0.14	40.68 \pm 0.59%	39.13 \pm 0.47

Table 7. Cross-validation performances of driving agents learned by GRPO.

	Val. Env.	RC \uparrow	Crash \downarrow	Reward \uparrow	Cost \downarrow
ADV-0 (w/ IPL)	Replay	0.713 \pm 0.016	0.177 \pm 0.019	45.55 \pm 2.21	0.55 \pm 0.01
	ADV-0	0.687 \pm 0.005	0.273 \pm 0.025	42.71 \pm 0.98	0.64 \pm 0.01
	CAT	0.695 \pm 0.004	0.250 \pm 0.022	44.50 \pm 0.63	0.60 \pm 0.02
	SAGE	0.670 \pm 0.015	0.270 \pm 0.016	42.49 \pm 2.16	0.60 \pm 0.02
	Rule	0.687 \pm 0.007	0.207 \pm 0.012	42.87 \pm 1.25	0.59 \pm 0.02
	Avg.	0.690 \pm 0.009	0.235 \pm 0.019	43.62 \pm 1.45	0.60 \pm 0.02
ADV-0 (w/o IPL)	Replay	0.694 \pm 0.027	0.183 \pm 0.025	42.20 \pm 3.21	0.61 \pm 0.04
	ADV-0	0.667 \pm 0.014	0.280 \pm 0.024	40.13 \pm 1.55	0.67 \pm 0.02
	CAT	0.667 \pm 0.019	0.267 \pm 0.026	39.99 \pm 2.01	0.67 \pm 0.03
	SAGE	0.661 \pm 0.028	0.240 \pm 0.008	40.28 \pm 3.31	0.63 \pm 0.04
	Heuristic	0.666 \pm 0.016	0.217 \pm 0.048	39.03 \pm 1.62	0.64 \pm 0.02
	Avg.	0.671 \pm 0.021	0.237 \pm 0.026	40.33 \pm 2.34	0.64 \pm 0.03
CAT	Replay	0.684 \pm 0.015	0.197 \pm 0.005	41.33 \pm 1.32	0.59 \pm 0.02
	ADV-0	0.641 \pm 0.022	0.293 \pm 0.042	37.84 \pm 1.29	0.69 \pm 0.00
	CAT	0.646 \pm 0.020	0.280 \pm 0.036	38.62 \pm 1.36	0.68 \pm 0.02
	SAGE	0.630 \pm 0.024	0.313 \pm 0.034	38.17 \pm 1.55	0.67 \pm 0.01
	Heuristic	0.630 \pm 0.029	0.273 \pm 0.033	36.57 \pm 1.75	0.67 \pm 0.01
	Avg.	0.646 \pm 0.022	0.271 \pm 0.030	38.51 \pm 1.45	0.66 \pm 0.01
Heuristic	Replay	0.694 \pm 0.031	0.190 \pm 0.010	41.45 \pm 3.01	0.61 \pm 0.02
	ADV-0	0.682 \pm 0.068	0.323 \pm 0.009	41.45 \pm 2.26	0.67 \pm 0.04
	CAT	0.684 \pm 0.022	0.310 \pm 0.021	41.89 \pm 2.18	0.68 \pm 0.04
	SAGE	0.661 \pm 0.073	0.357 \pm 0.014	40.20 \pm 1.98	0.67 \pm 0.01
	Heuristic	0.674 \pm 0.029	0.250 \pm 0.013	39.72 \pm 1.77	0.66 \pm 0.02
	Avg.	0.679 \pm 0.045	0.286 \pm 0.013	40.94 \pm 2.24	0.66 \pm 0.03
Replay	Replay	0.680 \pm 0.029	0.180 \pm 0.044	39.26 \pm 0.90	0.61 \pm 0.01
	ADV-0	0.635 \pm 0.042	0.308 \pm 0.050	36.64 \pm 3.20	0.69 \pm 0.01
	CAT	0.645 \pm 0.055	0.319 \pm 0.038	37.48 \pm 1.06	0.66 \pm 0.01
	SAGE	0.616 \pm 0.062	0.319 \pm 0.032	35.72 \pm 1.25	0.69 \pm 0.03
	Heuristic	0.637 \pm 0.047	0.264 \pm 0.047	35.77 \pm 3.46	0.69 \pm 0.02
	Avg.	0.643 \pm 0.047	0.278 \pm 0.042	36.97 \pm 1.97	0.67 \pm 0.02

Table 8. Cross-validation performances of driving agents learned by PPO.

	Val. Env.	RC \uparrow	Crash \downarrow	Reward \uparrow	Cost \downarrow
ADV-0 (w/ IPL)	Replay	0.707 \pm 0.018	0.193 \pm 0.015	45.56 \pm 0.87	0.56 \pm 0.02
	ADV-0	0.681 \pm 0.021	0.270 \pm 0.019	42.68 \pm 0.69	0.62 \pm 0.03
	CAT	0.690 \pm 0.010	0.260 \pm 0.029	43.65 \pm 1.54	0.60 \pm 0.04
	SAGE	0.678 \pm 0.008	0.268 \pm 0.023	43.60 \pm 1.37	0.59 \pm 0.03
	Heuristic	0.676 \pm 0.006	0.250 \pm 0.016	41.63 \pm 1.59	0.61 \pm 0.03
	Avg.	0.686 \pm 0.013	0.248 \pm 0.020	43.42 \pm 1.21	0.60 \pm 0.03
ADV-0 (w/o IPL)	Replay	0.696 \pm 0.010	0.188 \pm 0.018	44.80 \pm 1.01	0.59 \pm 0.01
	ADV-0	0.673 \pm 0.006	0.280 \pm 0.021	42.10 \pm 1.34	0.67 \pm 0.01
	CAT	0.677 \pm 0.009	0.275 \pm 0.047	42.62 \pm 2.00	0.67 \pm 0.01
	SAGE	0.670 \pm 0.013	0.263 \pm 0.013	42.96 \pm 1.80	0.63 \pm 0.03
	Heuristic	0.658 \pm 0.002	0.265 \pm 0.017	39.65 \pm 1.10	0.68 \pm 0.02
	Avg.	0.675 \pm 0.008	0.254 \pm 0.023	42.43 \pm 1.45	0.65 \pm 0.02
CAT	Replay	0.717 \pm 0.013	0.211 \pm 0.041	45.40 \pm 1.05	0.57 \pm 0.03
	ADV-0	0.666 \pm 0.023	0.330 \pm 0.071	40.52 \pm 1.85	0.66 \pm 0.03
	CAT	0.679 \pm 0.021	0.319 \pm 0.028	42.29 \pm 1.53	0.64 \pm 0.01
	SAGE	0.653 \pm 0.008	0.310 \pm 0.010	40.53 \pm 0.75	0.65 \pm 0.01
	Heuristic	0.676 \pm 0.012	0.270 \pm 0.030	41.49 \pm 0.70	0.62 \pm 0.01
	Avg.	0.678 \pm 0.015	0.288 \pm 0.036	42.05 \pm 1.18	0.63 \pm 0.02
Heuristic	Replay	0.608 \pm 0.038	0.210 \pm 0.020	37.08 \pm 0.91	0.66 \pm 0.02
	ADV-0	0.577 \pm 0.051	0.303 \pm 0.050	33.53 \pm 0.80	0.74 \pm 0.01
	CAT	0.593 \pm 0.010	0.278 \pm 0.015	35.79 \pm 2.10	0.70 \pm 0.02
	SAGE	0.593 \pm 0.008	0.270 \pm 0.012	36.02 \pm 2.00	0.70 \pm 0.02
	Heuristic	0.563 \pm 0.021	0.289 \pm 0.020	31.72 \pm 1.77	0.72 \pm 0.01
	Avg.	0.587 \pm 0.026	0.270 \pm 0.023	34.83 \pm 1.52	0.70 \pm 0.02
Replay	Replay	0.697 \pm 0.052	0.229 \pm 0.014	44.26 \pm 0.55	0.60 \pm 0.02
	ADV-0	0.629 \pm 0.035	0.420 \pm 0.030	38.32 \pm 1.33	0.73 \pm 0.02
	CAT	0.663 \pm 0.025	0.380 \pm 0.048	41.26 \pm 1.67	0.68 \pm 0.04
	SAGE	0.638 \pm 0.020	0.360 \pm 0.045	41.01 \pm 1.90	0.63 \pm 0.03
	Heuristic	0.620 \pm 0.019	0.381 \pm 0.032	36.63 \pm 1.00	0.72 \pm 0.02
	Avg.	0.649 \pm 0.030	0.354 \pm 0.034	40.30 \pm 1.29	0.67 \pm 0.03

Table 9. Cross-validation performances of driving agents learned by PPO-Lag.

	Val. Env.	RC \uparrow	Crash \downarrow	Reward \uparrow	Cost \downarrow
ADV-0 (w/ IPL)	Replay	0.676 \pm 0.012	0.142 \pm 0.015	44.82 \pm 1.20	0.53 \pm 0.01
	ADV-0	0.626 \pm 0.008	0.260 \pm 0.027	38.17 \pm 0.95	0.67 \pm 0.02
	CAT	0.647 \pm 0.013	0.250 \pm 0.027	40.80 \pm 1.11	0.64 \pm 0.02
	SAGE	0.632 \pm 0.014	0.271 \pm 0.018	39.61 \pm 1.83	0.65 \pm 0.02
	Rule	0.638 \pm 0.009	0.256 \pm 0.019	38.34 \pm 1.55	0.68 \pm 0.02
	Avg.	0.644 \pm 0.011	0.236 \pm 0.021	40.35 \pm 1.33	0.63 \pm 0.02
ADV-0 (w/o IPL)	Replay	0.605 \pm 0.022	0.178 \pm 0.028	33.08 \pm 2.55	0.74 \pm 0.03
	ADV-0	0.603 \pm 0.018	0.291 \pm 0.030	32.78 \pm 1.83	0.74 \pm 0.02
	CAT	0.603 \pm 0.023	0.272 \pm 0.035	32.56 \pm 2.14	0.74 \pm 0.03
	SAGE	0.585 \pm 0.020	0.260 \pm 0.025	31.85 \pm 2.84	0.72 \pm 0.04
	Heuristic	0.593 \pm 0.020	0.265 \pm 0.040	31.80 \pm 1.90	0.76 \pm 0.02
	Avg.	0.598 \pm 0.021	0.253 \pm 0.032	32.41 \pm 2.25	0.74 \pm 0.03
CAT	Replay	0.625 \pm 0.015	0.190 \pm 0.005	36.51 \pm 1.30	0.68 \pm 0.02
	ADV-0	0.599 \pm 0.022	0.305 \pm 0.042	32.91 \pm 1.25	0.75 \pm 0.01
	CAT	0.608 \pm 0.020	0.290 \pm 0.035	33.82 \pm 1.35	0.73 \pm 0.02
	SAGE	0.590 \pm 0.025	0.316 \pm 0.035	33.19 \pm 1.50	0.74 \pm 0.01
	Heuristic	0.604 \pm 0.028	0.286 \pm 0.033	33.09 \pm 1.70	0.71 \pm 0.01
	Avg.	0.605 \pm 0.022	0.277 \pm 0.030	33.90 \pm 1.42	0.72 \pm 0.01
Heuristic	Replay	0.630 \pm 0.030	0.202 \pm 0.010	36.82 \pm 3.00	0.69 \pm 0.02
	ADV-0	0.590 \pm 0.065	0.333 \pm 0.010	33.52 \pm 2.20	0.76 \pm 0.04
	CAT	0.606 \pm 0.022	0.324 \pm 0.020	34.27 \pm 2.15	0.75 \pm 0.04
	SAGE	0.586 \pm 0.070	0.354 \pm 0.015	32.56 \pm 2.00	0.76 \pm 0.01
	Heuristic	0.590 \pm 0.029	0.290 \pm 0.015	32.80 \pm 1.80	0.74 \pm 0.02
	Avg.	0.600 \pm 0.043	0.301 \pm 0.014	33.99 \pm 2.23	0.74 \pm 0.03
Replay	Replay	0.620 \pm 0.030	0.215 \pm 0.045	34.53 \pm 0.90	0.70 \pm 0.01
	ADV-0	0.570 \pm 0.040	0.364 \pm 0.050	30.20 \pm 3.20	0.78 \pm 0.01
	CAT	0.585 \pm 0.055	0.358 \pm 0.040	31.53 \pm 1.10	0.76 \pm 0.01
	SAGE	0.565 \pm 0.060	0.358 \pm 0.035	29.80 \pm 1.25	0.78 \pm 0.03
	Heuristic	0.581 \pm 0.045	0.320 \pm 0.045	30.50 \pm 3.40	0.77 \pm 0.02
	Avg.	0.584 \pm 0.046	0.323 \pm 0.043	31.31 \pm 1.97	0.76 \pm 0.02

Table 10. Cross-validation performances of driving agents learned by SAC.

	Val. Env.	RC \uparrow	Crash \downarrow	Reward \uparrow	Cost \downarrow
ADV-0 (w/ IPL)	Replay	0.781 \pm 0.011	0.130 \pm 0.016	53.66 \pm 1.02	0.41 \pm 0.01
	ADV-0	0.736 \pm 0.011	0.305 \pm 0.022	49.70 \pm 0.34	0.53 \pm 0.01
	CAT	0.745 \pm 0.013	0.268 \pm 0.024	50.48 \pm 1.02	0.52 \pm 0.03
	SAGE	0.745 \pm 0.016	0.250 \pm 0.025	48.84 \pm 1.79	0.51 \pm 0.04
	Heuristic	0.758 \pm 0.031	0.170 \pm 0.019	50.48 \pm 2.79	0.45 \pm 0.06
	Avg.	0.753 \pm 0.016	0.225 \pm 0.021	50.63 \pm 1.39	0.48 \pm 0.03
ADV-0 (w/o IPL)	Replay	0.784 \pm 0.020	0.160 \pm 0.022	54.40 \pm 1.69	0.44 \pm 0.03
	ADV-0	0.706 \pm 0.020	0.307 \pm 0.026	45.92 \pm 2.59	0.58 \pm 0.03
	CAT	0.729 \pm 0.011	0.287 \pm 0.026	47.81 \pm 1.48	0.58 \pm 0.03
	SAGE	0.743 \pm 0.027	0.260 \pm 0.024	49.35 \pm 2.73	0.50 \pm 0.05
	Heuristic	0.743 \pm 0.033	0.203 \pm 0.034	48.98 \pm 3.48	0.49 \pm 0.07
	Avg.	0.741 \pm 0.022	0.243 \pm 0.026	49.29 \pm 2.39	0.52 \pm 0.04
CAT	Replay	0.775 \pm 0.013	0.177 \pm 0.041	54.06 \pm 1.12	0.42 \pm 0.00
	ADV-0	0.698 \pm 0.010	0.353 \pm 0.034	45.81 \pm 0.57	0.60 \pm 0.03
	CAT	0.704 \pm 0.018	0.327 \pm 0.041	45.78 \pm 1.55	0.60 \pm 0.02
	SAGE	0.705 \pm 0.025	0.297 \pm 0.029	46.65 \pm 3.41	0.56 \pm 0.03
	Heuristic	0.727 \pm 0.024	0.247 \pm 0.038	47.48 \pm 2.57	0.53 \pm 0.04
	Avg.	0.722 \pm 0.018	0.280 \pm 0.037	47.96 \pm 1.84	0.54 \pm 0.02
Heuristic	Replay	0.718 \pm 0.030	0.200 \pm 0.028	47.20 \pm 4.13	0.54 \pm 0.07
	ADV-0	0.665 \pm 0.025	0.330 \pm 0.025	42.10 \pm 2.64	0.63 \pm 0.02
	CAT	0.672 \pm 0.024	0.320 \pm 0.022	42.50 \pm 2.84	0.64 \pm 0.03
	SAGE	0.670 \pm 0.030	0.295 \pm 0.030	42.30 \pm 3.77	0.60 \pm 0.05
	Heuristic	0.678 \pm 0.028	0.275 \pm 0.015	43.10 \pm 4.29	0.61 \pm 0.05
	Avg.	0.681 \pm 0.027	0.284 \pm 0.024	43.44 \pm 3.53	0.60 \pm 0.04
Replay	Replay	0.710 \pm 0.035	0.217 \pm 0.035	45.51 \pm 1.30	0.56 \pm 0.02
	ADV-0	0.625 \pm 0.045	0.360 \pm 0.046	37.81 \pm 2.50	0.67 \pm 0.03
	CAT	0.652 \pm 0.035	0.353 \pm 0.041	39.20 \pm 2.00	0.66 \pm 0.04
	SAGE	0.635 \pm 0.029	0.332 \pm 0.040	38.54 \pm 2.10	0.64 \pm 0.03
	Heuristic	0.638 \pm 0.027	0.316 \pm 0.035	39.09 \pm 2.50	0.65 \pm 0.01
	Avg.	0.652 \pm 0.034	0.316 \pm 0.039	40.03 \pm 2.08	0.64 \pm 0.03

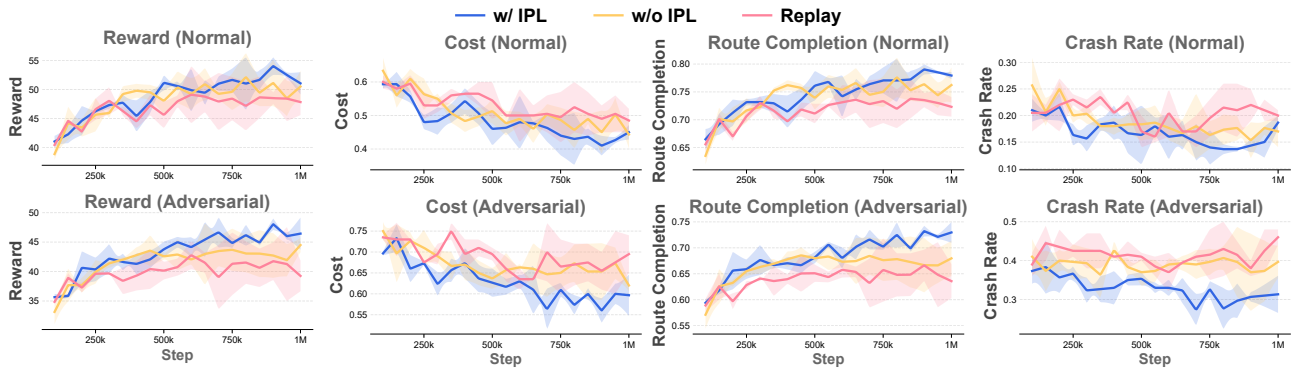


Figure 10. Learning curves of TD3.

Table 11. Cross-validation performances of driving agents learned by SAC-Lag.

	Val. Env.	RC \uparrow	Crash \downarrow	Reward \uparrow	Cost \downarrow
ADV-0 (w/ IPL)	Replay	0.787 \pm 0.006	0.127 \pm 0.017	54.62 \pm 0.26	0.40 \pm 0.02
	ADV-0	0.729 \pm 0.002	0.303 \pm 0.042	48.78 \pm 0.35	0.54 \pm 0.03
	CAT	0.725 \pm 0.011	0.297 \pm 0.019	48.01 \pm 1.10	0.57 \pm 0.02
	SAGE	0.736 \pm 0.007	0.250 \pm 0.024	48.88 \pm 0.58	0.52 \pm 0.01
	Heuristic	0.742 \pm 0.022	0.217 \pm 0.045	49.25 \pm 2.68	0.49 \pm 0.06
	Avg.	0.744 \pm 0.010	0.239 \pm 0.029	49.91 \pm 0.99	0.50 \pm 0.03
ADV-0 (w/o IPL)	Replay	0.776 \pm 0.009	0.135 \pm 0.025	53.75 \pm 1.29	0.42 \pm 0.02
	ADV-0	0.689 \pm 0.004	0.320 \pm 0.020	44.41 \pm 0.98	0.61 \pm 0.01
	CAT	0.699 \pm 0.002	0.320 \pm 0.000	45.36 \pm 0.43	0.61 \pm 0.03
	SAGE	0.707 \pm 0.009	0.260 \pm 0.030	46.63 \pm 0.19	0.56 \pm 0.02
	Heuristic	0.730 \pm 0.013	0.205 \pm 0.035	47.97 \pm 0.34	0.49 \pm 0.03
	Avg.	0.720 \pm 0.007	0.248 \pm 0.022	47.62 \pm 0.65	0.54 \pm 0.02
CAT	Replay	0.765 \pm 0.015	0.165 \pm 0.036	52.80 \pm 1.15	0.43 \pm 0.01
	ADV-0	0.685 \pm 0.012	0.345 \pm 0.035	44.55 \pm 0.61	0.61 \pm 0.03
	CAT	0.692 \pm 0.018	0.320 \pm 0.047	44.78 \pm 1.50	0.61 \pm 0.02
	SAGE	0.695 \pm 0.025	0.305 \pm 0.033	45.87 \pm 3.22	0.57 \pm 0.03
	Heuristic	0.712 \pm 0.024	0.255 \pm 0.042	46.50 \pm 2.52	0.54 \pm 0.04
	Avg.	0.710 \pm 0.019	0.278 \pm 0.039	46.90 \pm 1.80	0.55 \pm 0.03
Heuristic	Replay	0.731 \pm 0.030	0.193 \pm 0.024	48.36 \pm 4.17	0.53 \pm 0.07
	ADV-0	0.677 \pm 0.022	0.320 \pm 0.024	43.47 \pm 2.58	0.62 \pm 0.02
	CAT	0.686 \pm 0.024	0.313 \pm 0.021	43.81 \pm 2.86	0.63 \pm 0.03
	SAGE	0.687 \pm 0.027	0.283 \pm 0.031	43.61 \pm 3.71	0.59 \pm 0.05
	Heuristic	0.691 \pm 0.028	0.267 \pm 0.012	44.19 \pm 4.19	0.60 \pm 0.05
	Avg.	0.694 \pm 0.026	0.275 \pm 0.022	44.69 \pm 3.50	0.59 \pm 0.04
Heuristic	Replay	0.718 \pm 0.035	0.205 \pm 0.034	46.25 \pm 1.25	0.55 \pm 0.02
	ADV-0	0.635 \pm 0.047	0.355 \pm 0.045	38.80 \pm 2.55	0.66 \pm 0.03
	CAT	0.665 \pm 0.033	0.345 \pm 0.040	40.15 \pm 2.00	0.65 \pm 0.04
	SAGE	0.645 \pm 0.031	0.325 \pm 0.040	39.50 \pm 2.11	0.63 \pm 0.03
	Rule	0.650 \pm 0.029	0.305 \pm 0.036	39.80 \pm 2.54	0.64 \pm 0.01
	Avg.	0.663 \pm 0.035	0.307 \pm 0.039	40.90 \pm 2.09	0.63 \pm 0.03

Table 12. Cross-validation performances of driving agents learned by TD3.

	Val. Env.	RC \uparrow	Crash \downarrow	Reward \uparrow	Cost \downarrow
ADV-0 (w/ IPL)	Replay	0.787 \pm 0.002	0.187 \pm 0.031	53.15 \pm 0.76	0.43 \pm 0.01
	ADV-0	0.711 \pm 0.016	0.323 \pm 0.038	45.54 \pm 1.70	0.59 \pm 0.03
	CAT	0.724 \pm 0.016	0.300 \pm 0.029	46.67 \pm 1.55	0.58 \pm 0.02
	SAGE	0.734 \pm 0.016	0.267 \pm 0.046	47.69 \pm 1.52	0.53 \pm 0.05
	Heuristic	0.757 \pm 0.021	0.200 \pm 0.014	49.87 \pm 2.64	0.49 \pm 0.02
	Avg.	0.743 \pm 0.014	0.255 \pm 0.032	48.58 \pm 1.63	0.52 \pm 0.03
ADV-0 (w/o IPL)	Replay	0.761 \pm 0.031	0.160 \pm 0.024	50.21 \pm 2.09	0.44 \pm 0.01
	ADV-0	0.644 \pm 0.046	0.423 \pm 0.057	40.86 \pm 2.90	0.67 \pm 0.03
	CAT	0.689 \pm 0.036	0.373 \pm 0.077	45.46 \pm 2.04	0.59 \pm 0.05
	SAGE	0.669 \pm 0.049	0.337 \pm 0.068	41.95 \pm 3.39	0.62 \pm 0.05
	Heuristic	0.685 \pm 0.046	0.277 \pm 0.069	43.25 \pm 4.07	0.61 \pm 0.08
	Avg.	0.690 \pm 0.042	0.314 \pm 0.059	44.35 \pm 2.90	0.59 \pm 0.04
CAT	Replay	0.755 \pm 0.013	0.160 \pm 0.029	49.03 \pm 0.97	0.48 \pm 0.01
	ADV-0	0.668 \pm 0.017	0.367 \pm 0.033	42.60 \pm 0.23	0.65 \pm 0.02
	CAT	0.673 \pm 0.006	0.343 \pm 0.005	42.46 \pm 1.60	0.65 \pm 0.02
	SAGE	0.687 \pm 0.016	0.300 \pm 0.008	43.99 \pm 2.09	0.58 \pm 0.01
	Heuristic	0.706 \pm 0.009	0.237 \pm 0.029	45.21 \pm 0.88	0.56 \pm 0.03
	Avg.	0.698 \pm 0.012	0.281 \pm 0.021	44.66 \pm 1.15	0.58 \pm 0.02
Heuristic	Replay	0.713 \pm 0.030	0.210 \pm 0.016	45.57 \pm 3.01	0.52 \pm 0.02
	ADV-0	0.632 \pm 0.051	0.380 \pm 0.010	40.47 \pm 2.24	0.65 \pm 0.04
	CAT	0.661 \pm 0.022	0.320 \pm 0.020	42.40 \pm 2.18	0.61 \pm 0.04
	SAGE	0.654 \pm 0.045	0.315 \pm 0.015	42.51 \pm 1.99	0.63 \pm 0.01
	Heuristic	0.652 \pm 0.047	0.305 \pm 0.022	41.35 \pm 1.85	0.60 \pm 0.02
	Avg.	0.662 \pm 0.039	0.306 \pm 0.017	42.46 \pm 2.25	0.60 \pm 0.03
Replay	Replay	0.727 \pm 0.026	0.210 \pm 0.010	47.77 \pm 3.00	0.51 \pm 0.07
	ADV-0	0.638 \pm 0.019	0.435 \pm 0.005	39.01 \pm 2.08	0.67 \pm 0.02
	CAT	0.643 \pm 0.038	0.455 \pm 0.015	39.96 \pm 3.15	0.69 \pm 0.04
	SAGE	0.654 \pm 0.035	0.340 \pm 0.050	41.54 \pm 2.42	0.59 \pm 0.04
	Heuristic	0.700 \pm 0.020	0.280 \pm 0.010	45.02 \pm 1.55	0.56 \pm 0.01
	Avg.	0.672 \pm 0.028	0.344 \pm 0.018	42.66 \pm 2.44	0.60 \pm 0.04

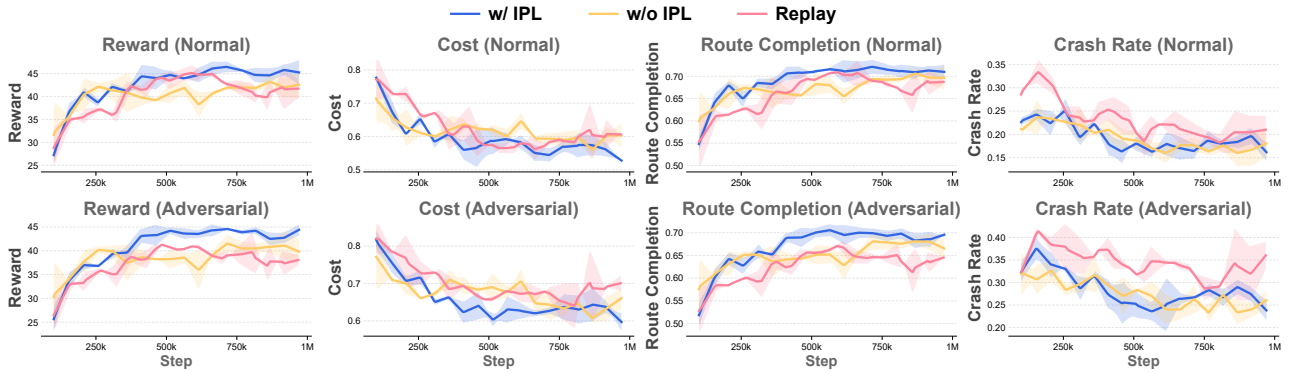


Figure 11. Learning curves of GRPO.

Table 13. Performance comparison of learning-based planners before and after adversarial fine-tuning using ADV-0 (GRPO).

Model Phase	Val. Env.	RC \uparrow	Crash \downarrow	Reward \uparrow	Cost \downarrow
PlanTF (Pretrained)	Replay	0.727 \pm 0.021	0.220 \pm 0.027	41.53 \pm 3.10	0.76 \pm 0.03
	ADV-0	0.581 \pm 0.030	0.420 \pm 0.035	32.11 \pm 2.54	1.24 \pm 0.05
	CAT	0.615 \pm 0.025	0.385 \pm 0.030	35.26 \pm 2.16	1.09 \pm 0.03
	SAGE	0.595 \pm 0.028	0.407 \pm 0.032	33.80 \pm 2.80	1.15 \pm 0.04
	Heuristic	0.620 \pm 0.020	0.352 \pm 0.032	36.53 \pm 1.97	0.94 \pm 0.03
	Avg.	0.628 \pm 0.025	0.357 \pm 0.031	35.85 \pm 2.51	1.04 \pm 0.04
PlanTF (Fine-tuned)	Replay	0.738 \pm 0.015	0.199 \pm 0.018	46.20 \pm 1.88	0.62 \pm 0.02
	ADV-0	0.655 \pm 0.012	0.293 \pm 0.022	40.80 \pm 1.20	0.85 \pm 0.00
	CAT	0.668 \pm 0.010	0.273 \pm 0.020	42.11 \pm 1.16	0.78 \pm 0.01
	SAGE	0.640 \pm 0.018	0.305 \pm 0.025	39.50 \pm 1.56	0.88 \pm 0.03
	Heuristic	0.671 \pm 0.024	0.246 \pm 0.038	41.28 \pm 2.32	0.72 \pm 0.05
	Avg.	0.674 \pm 0.016	0.263 \pm 0.025	41.98 \pm 1.62	0.77 \pm 0.02
Average Relative Change		+7.46%	-26.23%	+17.11%	-25.68%
SMART (Pretrained)	Replay	0.686 \pm 0.020	0.255 \pm 0.023	38.59 \pm 3.51	0.83 \pm 0.05
	ADV-0	0.540 \pm 0.035	0.460 \pm 0.049	29.80 \pm 2.99	1.35 \pm 0.04
	CAT	0.565 \pm 0.031	0.433 \pm 0.033	31.50 \pm 2.43	1.23 \pm 0.05
	SAGE	0.556 \pm 0.032	0.448 \pm 0.038	30.27 \pm 3.10	1.30 \pm 0.04
	Heuristic	0.586 \pm 0.029	0.384 \pm 0.026	33.16 \pm 2.20	1.05 \pm 0.07
	Avg.	0.587 \pm 0.029	0.396 \pm 0.034	32.66 \pm 2.85	1.15 \pm 0.05
SMART (Fine-tuned)	Replay	0.705 \pm 0.010	0.230 \pm 0.026	42.13 \pm 2.11	0.77 \pm 0.01
	ADV-0	0.610 \pm 0.018	0.340 \pm 0.022	36.51 \pm 1.56	0.97 \pm 0.02
	CAT	0.625 \pm 0.012	0.313 \pm 0.022	37.82 \pm 1.40	0.95 \pm 0.03
	SAGE	0.595 \pm 0.020	0.352 \pm 0.028	35.20 \pm 1.82	1.05 \pm 0.03
	Heuristic	0.620 \pm 0.016	0.292 \pm 0.018	37.57 \pm 1.63	0.85 \pm 0.03
	Avg.	0.631 \pm 0.015	0.305 \pm 0.023	37.85 \pm 1.70	0.92 \pm 0.02
Average Relative Change		+7.57%	-22.88%	+15.86%	-20.31%

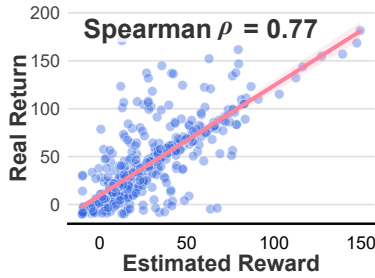


Figure 12. **Validation of proxy reward estimator.** Comparison of the estimated returns against the ground-truth. The strong Spearman correlation ($\rho = 0.77$) suggests that our rule-based proxy effectively preserves the preference ranking of adversarial candidates.

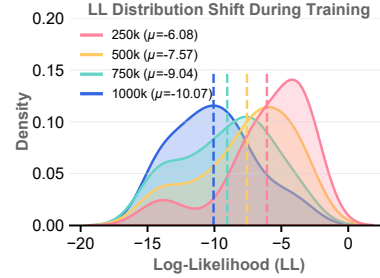


Figure 13. **Evolution of the adversary distribution.** Likelihood of adversarial trajectories at different training steps. As the ego improves, the distribution shifts towards lower values, suggesting that ADV-0 actively identifies nonstationary failure boundary.

Table 14. **Detailed breakdown of the trajectory-level reward model values.** Values represent the average accumulated discounted reward (over a 2.0s horizon with discount factor $\gamma = 0.99$) of the *best* planned trajectory selected by the model across all validation steps. **Reward components & weights:** **Progress** ($w_{\text{prog}} = 1.0$, longitudinal advance), **Collision** ($w_{\text{coll}} = 20.0$, penalty for overlap with objects), **Off-road** ($w_{\text{off}} = 5.0$, penalty for lane deviation), **Comfort** ($w_{\text{acc}} = 0.1$, $w_{\text{jerk}} = 0.1$, penalties for harsh dynamics), **Speed Efficiency** ($w_{\text{eff}} = 0.2$, penalty for deviating from 10m/s). Note that the negative improvement in Speed Efficiency reflects a safety-efficiency trade-off, where the fine-tuned planner adopts a more conservative velocity profile to satisfy safety constraints.

Method	Progress (+)	Collision (-)	Off-road (-)	Comfort (-)	Speed Eff. (-)	Total Score
PlanTF (Pretrained)	14.17 \pm 1.53	-2.85 \pm 0.92	-0.12 \pm 0.05	-0.34 \pm 0.08	-0.54 \pm 0.12	10.32 \pm 1.79
PlanTF (Fine-tuned)	16.45 \pm 0.85	-0.89 \pm 0.45	-0.05 \pm 0.04	-0.24 \pm 0.05	-0.64 \pm 0.13	14.63 \pm 0.97
Improvement	+16.09%	+68.77%	+58.33%	+29.41%	-18.52%	+41.76%
SMART (Pretrained)	13.20 \pm 1.80	-3.61 \pm 1.11	-0.25 \pm 0.08	-1.26 \pm 0.25	-0.60 \pm 0.15	7.48 \pm 2.14
SMART (Fine-tuned)	15.10 \pm 1.10	-1.75 \pm 0.37	-0.17 \pm 0.05	-0.92 \pm 0.19	-0.65 \pm 0.11	11.61 \pm 1.18
Improvement	+14.39%	+51.52%	+32.00%	+26.98%	-8.33%	+55.21%

Table 15. Full results of quantitative evaluation on the unbiased long-tailed set mined from real-world data. The benchmark consists of four long-tail scenario categories filtered by strict physical thresholds: *Critical TTC* (min TTC < 0.4s), *Critical PET* (PET < 1.0s), *Hard Dynamics* (Longitudinal Acc < $-4.0m/s^2$ or $|Jerk| > 4.0m/s^3$), and *Rare Cluster* (topologically sparse trajectory clusters). **Reactive Traffic** denotes whether background vehicles utilize IDM/MOBIL policies to interact with the agent (✓) or strictly follow logged trajectories (×). Metrics assess **Safety Margin** (higher values indicate earlier risk detection), **Stability & Comfort** (lower Jerk indicates smoother control), and **Defensive Driving** performance, quantified by Near-Miss Rate (hazardous proximity without collision) and RDP Violation (percentage of time requiring deceleration > $6m/s^2$ to avoid collision).

Scenario Category	Percentage	Reactive Traffic	Safety Margin		Stability & Comfort		Defensive Driving		
			Avg Min-TTC (↑)	Avg Min-PET (↑)	Mean Abs Jerk (↓)	95% Jerk (↓)	Near-Miss Rate (↓)	RDP Violation Rate (↓)	
ADV-O (w/ IPL)	Critical TTC	7.40%	0.645 ± 0.122	1.450 ± 0.50	1.853 ± 0.188	5.850 ± 1.252	65.28% ± 1.45%	15.53% ± 4.16%	
	Critical PET	3.40%	0.492 ± 0.025	1.150 ± 0.20	1.623 ± 0.095	5.157 ± 0.653	74.57% ± 5.52%	58.26% ± 3.29%	
	Hard Dynamics	3.20%	✓	0.885 ± 0.157	N/A	1.685 ± 0.250	4.555 ± 0.951	55.40% ± 8.26%	29.54% ± 4.80%
	Rare Cluster	5.20%		1.951 ± 0.450	0.850 ± 0.25	1.451 ± 0.143	4.650 ± 0.684	58.55% ± 2.12%	31.48% ± 2.81%
	Avg			0.993 ± 0.189	1.150 ± 0.317	1.653 ± 0.169	5.053 ± 0.885	63.45% ± 4.34%	33.70% ± 3.77%
	Critical TTC	7.40%		0.658 ± 0.130	1.410 ± 0.48	1.812 ± 0.165	5.784 ± 1.102	62.15% ± 1.32%	14.80% ± 3.83%
	Critical PET	3.40%	×	2.550 ± 0.036	1.080 ± 0.22	1.651 ± 0.117	5.923 ± 0.823	68.40% ± 4.86%	65.13% ± 2.56%
	Hard Dynamics	3.20%		0.850 ± 0.140	N/A	1.525 ± 0.380	4.421 ± 1.259	58.11% ± 7.52%	30.23% ± 3.50%
	Rare Cluster	5.20%		2.051 ± 0.422	0.820 ± 0.24	1.480 ± 0.155	4.580 ± 0.626	55.23% ± 2.05%	35.63% ± 1.51%
	Avg			1.527 ± 0.182	1.103 ± 0.313	1.617 ± 0.204	5.177 ± 0.953	60.97% ± 3.94%	36.45% ± 2.85%
CAT	Critical TTC	7.40%		0.465 ± 0.058	1.350 ± 0.45	2.123 ± 0.245	6.726 ± 1.064	81.98% ± 3.12%	24.46% ± 3.47%
	Critical PET	3.40%	✓	0.411 ± 0.021	0.950 ± 0.25	1.653 ± 0.108	4.706 ± 0.405	91.67% ± 3.61%	73.20% ± 8.84%
	Hard Dynamics	3.20%		0.573 ± 0.137	N/A	1.889 ± 0.271	4.985 ± 0.706	85.42% ± 9.55%	41.04% ± 7.71%
	Rare Cluster	5.20%		1.850 ± 0.55	0.750 ± 0.25	1.834 ± 0.292	5.271 ± 1.155	73.08% ± 7.69%	40.48% ± 4.46%
	Avg			0.825 ± 0.192	1.017 ± 0.317	1.875 ± 0.229	5.422 ± 0.833	83.04% ± 5.99%	44.80% ± 6.12%
	Critical TTC	7.40%		0.469 ± 0.058	1.310 ± 0.40	2.168 ± 0.206	6.871 ± 1.149	81.08% ± 4.68%	24.82% ± 3.54%
	Critical PET	3.40%	×	2.850 ± 1.10	0.910 ± 0.30	1.818 ± 0.085	5.876 ± 0.869	75.00% ± 12.50%	87.97% ± 4.17%
	Hard Dynamics	3.20%		0.559 ± 0.091	N/A	1.960 ± 0.299	5.232 ± 0.886	81.25% ± 6.25%	44.03% ± 5.88%
	Rare Cluster	5.20%		1.780 ± 0.60	0.720 ± 0.28	1.969 ± 0.182	6.028 ± 0.820	64.10% ± 8.01%	47.96% ± 5.38%
	Avg			1.415 ± 0.462	0.980 ± 0.327	1.979 ± 0.193	6.002 ± 0.931	75.36% ± 7.86%	51.20% ± 4.74%
Heuristic	Critical TTC	7.40%		0.513 ± 0.066	1.550 ± 0.60	2.252 ± 0.101	6.849 ± 0.698	81.98% ± 1.56%	25.73% ± 1.89%
	Critical PET	3.40%	✓	0.404 ± 0.039	1.100 ± 0.50	1.957 ± 0.316	6.204 ± 0.577	85.42% ± 3.61%	81.71% ± 6.07%
	Hard Dynamics	3.20%		0.938 ± 0.244	N/A	2.151 ± 0.308	6.353 ± 1.384	62.50% ± 16.54%	41.41% ± 5.35%
	Rare Cluster	5.20%		1.600 ± 0.45	0.800 ± 0.30	2.155 ± 0.224	6.761 ± 1.107	67.95% ± 2.22%	46.31% ± 1.31%
	Avg			0.864 ± 0.200	1.150 ± 0.467	2.129 ± 0.237	6.542 ± 0.942	74.46% ± 5.98%	48.79% ± 3.65%
	Critical TTC	7.40%		0.503 ± 0.061	1.480 ± 0.55	2.229 ± 0.054	6.945 ± 0.891	79.28% ± 4.13%	26.07% ± 2.60%
	Critical PET	3.40%	×	3.550 ± 1.50	1.050 ± 0.45	2.103 ± 0.171	6.449 ± 0.485	75.00% ± 12.50%	88.02% ± 2.03%
	Hard Dynamics	3.20%		0.833 ± 0.190	N/A	2.098 ± 0.358	6.444 ± 1.220	64.58% ± 7.22%	43.71% ± 0.52%
	Rare Cluster	5.20%		1.520 ± 0.40	0.750 ± 0.35	2.366 ± 0.288	7.273 ± 1.668	56.41% ± 12.36%	50.61% ± 1.95%
	Avg			1.601 ± 0.538	1.093 ± 0.450	2.199 ± 0.218	6.778 ± 1.066	68.82% ± 9.05%	52.10% ± 1.77%
Replay	Critical TTC	7.40%		0.355 ± 0.045	0.950 ± 0.35	2.855 ± 0.359	8.553 ± 2.101	94.28% ± 2.51%	55.69% ± 6.27%
	Critical PET	3.40%	✓	0.282 ± 0.015	0.650 ± 0.15	2.555 ± 0.427	7.857 ± 1.259	96.86% ± 1.56%	92.54% ± 1.85%
	Hard Dynamics	3.20%		0.453 ± 0.124	N/A	2.951 ± 0.550	8.200 ± 1.655	85.49% ± 9.55%	68.23% ± 8.46%
	Rare Cluster	5.20%		1.257 ± 0.555	0.450 ± 0.15	2.753 ± 0.387	8.450 ± 1.858	81.50% ± 3.59%	62.47% ± 4.50%
	Avg			0.587 ± 0.185	0.683 ± 0.217	2.779 ± 0.431	8.265 ± 1.718	89.53% ± 4.30%	69.73% ± 5.27%
	Critical TTC	7.40%		0.389 ± 0.050	1.050 ± 0.40	2.653 ± 0.281	8.159 ± 1.806	91.51% ± 2.11%	52.45% ± 5.58%
	Critical PET	3.40%	×	1.855 ± 1.204	0.720 ± 0.18	2.481 ± 0.357	7.620 ± 0.956	88.56% ± 4.25%	90.18% ± 2.11%
	Hard Dynamics	3.20%		0.481 ± 0.112	N/A	2.825 ± 0.485	7.950 ± 1.458	82.15% ± 8.81%	65.57% ± 7.25%
	Rare Cluster	5.20%		1.188 ± 0.483	0.420 ± 0.12	2.922 ± 0.410	8.688 ± 1.928	78.29% ± 3.16%	65.82% ± 3.80%
	Avg			0.978 ± 0.462	0.730 ± 0.233	2.720 ± 0.383	8.104 ± 1.537	85.13% ± 4.58%	68.50% ± 4.68%

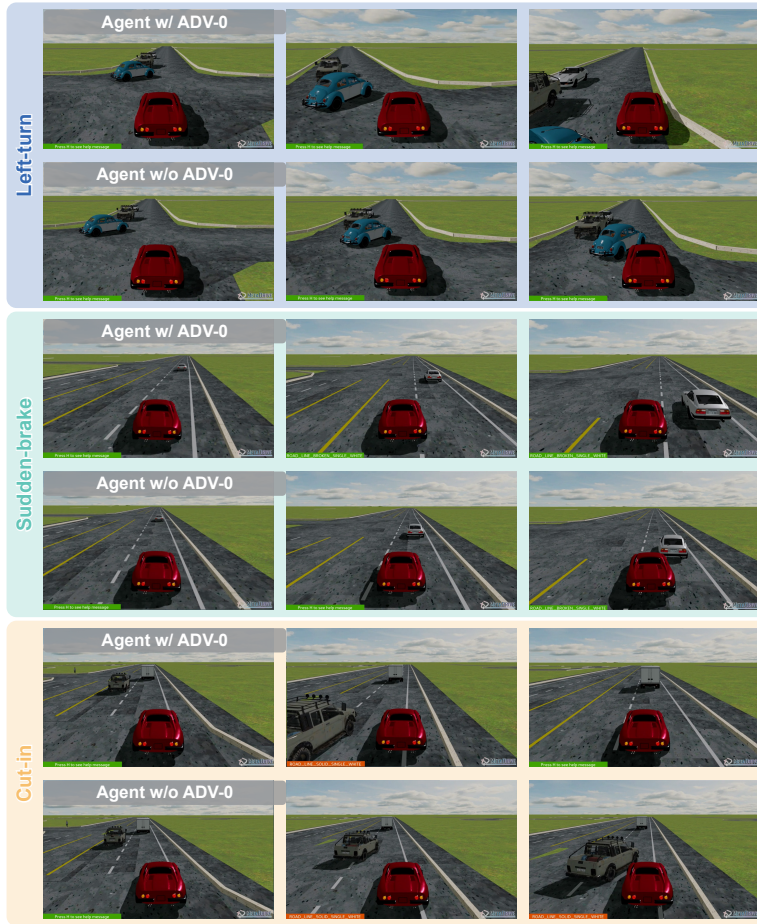


Figure 14. **Qualitative comparison of improved safe driving ability after being trained with ADV-0.** We showcase three typical safety-critical scenarios generated by the adversary: Left-turn, Sudden-brake, and Cut-in. In each column, the bottom row (Agent w/o ADV-0) shows the baseline agent failing to anticipate the aggressive behavior of the background traffic, resulting in collisions. In contrast, the top row (Agent w/ ADV-0) demonstrates that the agent trained with our framework learns robust defensive behaviors, such as yielding at intersections or decelerating in time, thereby successfully avoiding accidents.

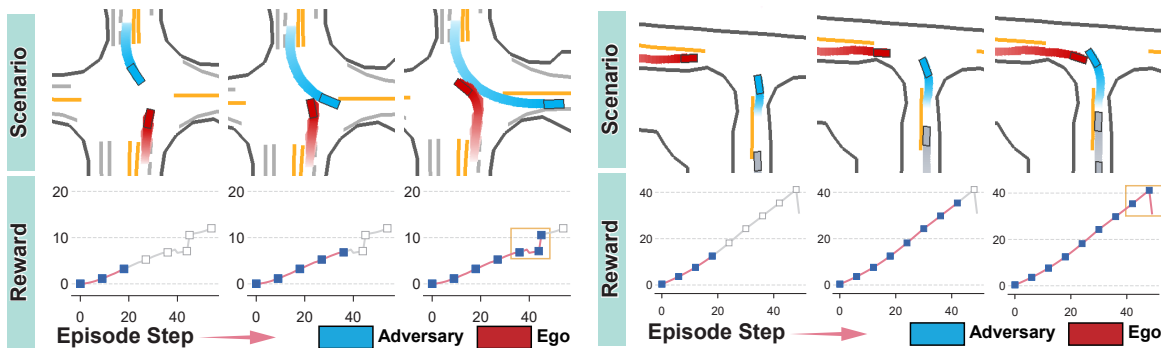


Figure 15. **Additional qualitative examples of reward-reduced adversarial scenarios from ADV-0.** In the first case (left), the adversary interrupts the straight-going ego, forcing it to deviate from the lane centerline to avoid a crash; this maneuver halts the ego’s progress, causing the cumulative reward to stagnate. In the second case (right), a collision occurs near the end of the episode, triggering a sharp drop in the cumulative reward due to the safety penalty.

D. Detailed Experimental Setups

In this section, we provide a comprehensive description of the experimental environment, datasets, baseline methods, model implementations, and hyperparameter configurations used in our study. Our experimental design follows the protocols established in prior works (Zhang et al., 2023; Nie et al., 2025; Stoler et al., 2025) to ensure a fair and rigorous comparison.

D.1. Environment and Dataset

Waymo Open Motion Dataset (WOMD). We utilize the WOMD as the source of real-world traffic scenarios. WOMD is a large-scale dataset containing diverse and complex urban driving environments captured in various conditions. Each scenario spans 9 seconds and is sampled at 10 Hz, capturing complex interactions between vehicles, pedestrians, and cyclists. Following the standard practices in safety-critical scenario generation, we filter and select a subset of 500 scenarios that involve interactive and complex behaviors.

MetaDrive simulator. All experiments are conducted within the MetaDrive simulator (Li et al., 2022), a lightweight and efficient platform that supports importing real-world data for closed-loop simulation. MetaDrive constructs the static map environment and replays the background traffic trajectories based on the WOMD logs. The simulation runs at a frequency of 10 Hz. The observation space consists of the ego vehicle’s kinematic state (velocity, steering, heading), navigation information (relative distance and direction to references), and surrounding information (surrounding traffic, road boundaries, and road lines) encoded as a vector by a simulated 2D LiDAR with 30 lasers and a 50-meter detection range. The action space consists of low-level continuous control signals including steering, brake, and throttle.

Reward definition. The ground-truth reward function for the ego agent is designed to balance safety and progression. It is composed of a dense driving reward and sparse terminal penalties. Formally, the reward function R_t at step t is defined as:

$$R_t = R_{\text{driving}} + R_{\text{success}} - P_{\text{collision}} - P_{\text{offroad}} \quad (48)$$

where $R_{\text{driving}} = d_t - d_{t-1}$ represents the longitudinal progress along the reference route, incentivizing the agent to move toward the destination. $R_{\text{success}} = +10$ is a sparse reward granted upon reaching the destination. Safety penalties are applied for terminal failures: $P_{\text{crash}} = 10$ for collisions with vehicles or objects, and $P_{\text{out}} = 10$ for driving out of the drivable road boundaries. Additionally, a small speed reward of $0.1 \times v_t$ is added to encourage movement. The episode terminates if the agent succeeds, crashes, or leaves the drivable area. For Lagrangian-based algorithms (e.g., PPO-Lag), we define a binary cost function C_t which equals 1 if a safety violation occurs and 0 otherwise.

D.2. Detailed Implementation

D.2.1. PROXY REWARD ESTIMATOR

To efficiently estimate the ego’s expected return $\hat{J}(Y^{\text{Adv}}, \pi_\theta)$ without executing computationally expensive closed-loop simulations during the inner loop, we implement a vectorized rule-based proxy evaluator. This module calculates the geometric interaction between a candidate adversarial trajectory Y^{Adv} and a sampled ego response Y^{Ego} from the cached history buffer. Let $Y^{\text{Ego}} = \{p_t^{\text{ego}}, \psi_t^{\text{ego}}\}_{t=1}^T$ and $Y^{\text{Adv}} = \{p_t^{\text{adv}}, \psi_t^{\text{adv}}\}_{t=1}^T$ denote the sequences of position and yaw for the ego and adversary, respectively. The proxy reward is calculated by mimicking the scheme in MetaDrive (Eq. 48):

Collision detection. We approximate the vehicle geometry using Oriented Bounding Boxes (OBB) defined by the center position, yaw, length l , and width w . For each timestep t , we compute the four corner coordinates of both vehicles. We employ the Separating Axis Theorem (SAT) to determine if the two OBBs overlap. A collision penalty r_{crash} is applied if an overlap is detected at any timestep, and the evaluation terminates early.

Route progress and termination. We map the ego’s position to the Frenet frame of the reference lane to obtain the longitudinal coordinate s_t and lateral deviation d_t . The evaluation terminates if: (1) *Success*: the longitudinal progress $s_t/L_{\text{total}} > 0.95$, granting a reward r_{success} . (2) *Off-road*: the lateral deviation $|d_t| > 10.0$ meters, applying a penalty r_{offroad} .

Dense reward. If no termination condition is met, a dense driving reward is accumulated based on the incremental longitudinal progress $\Delta s_t = s_t - s_{t-1}$. The total estimated return is the sum of step-wise rewards and terminal bonuses/penalties:

$$\mathcal{R}_{\text{proxy}} = \sum_{t=1}^{T_{\text{end}}} (\lambda_{\text{drive}} \cdot \Delta s_t) + \mathbb{I}_{\text{crash}} \cdot r_{\text{crash}} + \mathbb{I}_{\text{success}} \cdot r_{\text{success}} + \mathbb{I}_{\text{offroad}} \cdot r_{\text{offroad}}. \quad (49)$$

Once a terminal condition is met, the summation stops, and the cumulative value is returned. This geometric calculation is fully vectorized across the batch of candidate trajectories, allowing for rapid evaluation of potential attacks. In our experiments, we set $r_{\text{success}} = 10$, $r_{\text{crash}} = -10$, $r_{\text{offroad}} = -10$, and $\lambda_{\text{drive}} = 1.0$.

Baseline schemes. For the ablation study in Figure 8, we compare against: (1) *Experience*: We query the ego’s replay buffer. If the exact scenario context exists, we use the recorded return; otherwise, we retrieve the return of the nearest neighbor scenario based on trajectory similarity. (2) *RewardModel*: We train a separate learnable reward model $\mathcal{M}(X, Y^{\text{Ego}}, Y^{\text{Adv}})$ via supervised regression on the historical interaction dataset to predict the scalar return. (3) *GTReward*: We execute the physics engine in a parallel process to roll out the interaction between π_θ and the specific Y^{Adv} to obtain the exact return. While our results suggest that rule-based approach is effective, future work could explore integrating value function approximations (e.g., Q-networks from Actor-Critic architecture) to estimate returns for more complex reward functions.

Context-aware buffer. As noted in Section 3.2, the validity of the rule-based proxy estimator relies on the geometric consistency between the adversarial candidate Y^{Adv} and the ego response Y^{Ego} . Since different scenarios possess distinct map topologies and coordinate systems, using a global history buffer would lead to physically meaningless calculations. To address this, we implement the ego history buffer \mathcal{H}_{ego} as a context-indexed dictionary, mapping each unique scenario ID to a First-In-First-Out (FIFO) queue of its historical ego trajectories: $\mathcal{H}_{\text{ego}}(X) = \{Y_i^{\text{Ego}} | X\}_{i=1}^N$. This ensures that the geometric interaction $R_{\text{proxy}}(Y^{\text{Ego}}, Y^{\text{Adv}})$ is always computed between trajectories residing in the same spatial environment.

A key challenge raised by the dynamic training process is handling newly sampled contexts X_{new} that have not yet been interacted with by the current ego policy, resulting in an empty buffer $\mathcal{H}_{\text{ego}}(X_{\text{new}}) = \emptyset$. To address this, we employ a warm-up rollout before the inner-loop adversarial update begins for a sampled batch of contexts: (1) We check the buffer status for each context X in the batch. (2) If $\mathcal{H}_{\text{ego}}(X_{\text{new}}) = \emptyset$, we execute a single inference rollout of the current ego policy π_θ in the simulator. Importantly, this rollout is conducted against the non-adversarial replay log. (3) The resulting trajectory $Y_{\text{ref}}^{\text{Ego}}$ represents the ego’s baseline behavior in the absence of attacks and is added to $\mathcal{H}_{\text{ego}}(X)$. This mechanism ensures that the proxy estimator always has a valid reference to approximate the ego’s vulnerability, even for unseen scenarios. In addition, the proxy estimator always calculates geometric interactions between trajectories sharing the same spatial topology. As the training progresses, new interactions under adversarial perturbations are generated and added to the buffer, gradually shifting the distribution in $\mathcal{H}_{\text{ego}}(X)$ from naturalistic responses to defensive responses against attacks.

D.2.2. EVALUATION AND BENCHMARK

Adversarial scenario generation. We follow the safety-critical scenario generation evaluation protocol used in Zhang et al. (2023). For each scenario, the evaluation presented in Table 1 and Table 6 follows a two-stage process: (1) The environment is reset with a fixed seed and the ego agent first interacts with the log-replayed environment to generate a reference trajectory; (2) The adversarial generator conditions on the context and the ego’s reference trajectory to generate adversarial trajectories for one selected adversary (which is marked as `Object-of-Interests` in WOMB). This trajectory is set as a fixed plan for the adversary traffic in the simulator. For ADV-0, we employ a worst-case sampling strategy for evaluation, setting the sampling temperature $\tau \rightarrow 0$ (Eq. 6) to select the trajectory with the highest estimated adversarial utility from $K = 32$ candidates. We test against three kinds of driving policies: a *Replay* policy that follows ground truth logs from WOMB, an *IDM* policy representing reactive rule-based drivers, and *RL agents* trained via standard PPO on replay logs. These systems under test execute their control loop in the environment. The primary metrics are Collision Rate (CR), defined as the percentage of episodes where the ego collides with the adversary, and Ego’s Return (ER), the cumulative reward achieved by the ego. For the baselines adversarial generators, we utilize their official implementations but adapt them for our evaluation environment to ensure a fair comparison. All of them follow the same evaluation procedure. For the realism penalty metric in Figure 9, we adopt the trajectory-level measure from Nie et al. (2025), which discourages trajectories that are physically implausible or exhibit unnatural driving behavior.

Performance validation of learned agents. To rigorously evaluate the generalizability of the learned AD policies and compare different adversarial learning methods, we established a cross-validation protocol where each trained agent is tested against multiple distinct scenario generators. For the evaluation, we utilized a held-out test set of 100 WOMD scenarios that were not seen during training. We compared five types of agents: those adversarially trained by ADV-0 (with and without IPL), CAT, *Heuristic*, and a baseline trained solely on *Replay* data. All these agents are trained using 400 WOMD scenarios. Each agent was evaluated in five distinct environments with the held-out test set: *Replay*, ADV-0, CAT, SAGE, and *Heuristic*. Note that since SAGE introduces an additional scenario difficulty training curriculum, we exclude it for training methods. For each evaluation run, we used agents saved at the best validation checkpoints and recorded four metrics: Route Completion (RC), Crash Rate (percentage of episodes ending in collision), Reward (cumulative environmental reward), and Cost (safety violation penalty). To ensure statistical significance, the reported results in Table 2 are averaged across 6 different underlying RL algorithms (GRPO, PPO, PPO-Lag, SAC, SAC-Lag, TD3) and multiple random seeds. For the specific cross-validation in Table 3, we utilized the TD3 agent and compared the relative performance change when the adversary is enhanced with IPL versus a pretrained prior equipped with energy-based sampling (Eq. 6).

Evaluation in long-tailed scenarios. Generated scenarios from adversarial models can be biased and cause a sim-to-real gap for AD policies. To ensure an unbiased evaluation of policy robustness, we construct a curated evaluation set by mining additional 500 held-out scene segments from the WOMD. These scenarios are not shown in the training set. We employ strict physical thresholds to identify and categorize rare, safety-critical events: (1) *Critical TTC*: scenarios containing frames where the TTC between the ego and any object drops below $0.4s$; (2) *Critical PET*: scenarios with a Post-Encroachment Time (PET) lower than $1.0s$, indicating high-risk intersection crossings; (3) *Hard Dynamics*: scenarios involving aggressive behaviors, defined by longitudinal deceleration exceeding $-4.0m/s^2$ or absolute jerk exceeding $4.0m/s^3$; and (4) *Rare Cluster*: scenarios belonging to the two lowest-density clusters identified via K-Means clustering ($k = 10$) on trajectory features for all interacting objects, including curvature, velocity profiles, and displacement. During evaluation, we reproduce these scenarios in the simulator and utilize two traffic modes: a non-reactive mode where background vehicles follow logged trajectories, and a reactive mode where vehicles are controlled by IDM and MOBIL policies to simulate human-like interaction with the agent. In addition to safety margin and stability metrics, we also report *Near-Miss Rate*, defined as the percentage of episodes where $TTC < 1.0s$ or distance $< 0.5m$ without collision, and *RDP Violation*, which measures the frequency of violating the Responsibility-Sensitive Safety (RSS) Danger Priority safety distances.

D.2.3. ADAPTABILITY TO DIFFERENT RL ALGORITHMS

This section elaborates on the implementation details regarding the integration of ADV-0 with various RL algorithms, as mentioned in Section 3.1. We specifically address the synchronization mechanisms and the specialized credit assignment strategy developed for critic-free architectures to ensure stable convergence in safety-critical tasks.

RL algorithms. Our framework is designed to be algorithm-agnostic, treating the adversarial generator as a dynamic component of the environment dynamics \mathcal{P}_ψ . Consequently, the ego agent perceives the generated adversarial trajectories simply as state transitions, allowing ADV-0 to support both on-policy and off-policy algorithms. In our experiments, we instantiate the ego policy using six distinct algorithms, covering both on-policy and off-policy paradigms, as well as Lagrangian variants for constrained optimization: GRPO, PPO, SAC, TD3, PPO-Lag, and SAC-Lag. The primary distinction in implementation lies in the data collection and update scheduling. For *on-policy* methods (e.g., PPO, GRPO), the training alternates strictly between the adversary and the defender. In the outer loop, we fix the adversary ψ and collect a batch of trajectories \mathcal{B} using the current ego policy π_θ . The policy is updated using this batch, which is then discarded to ensure that the policy gradient is estimated using the data distribution induced by the current adversary. Conversely, for *off-policy* methods (e.g., SAC, TD3), we maintain a replay buffer \mathcal{D} . While the adversary ψ evolves periodically, older transitions in \mathcal{D} technically become off-dynamics data. To mitigate the impact of non-stationarity, we employ a sliding window approach where the replay buffer has a limited capacity, ensuring that the value function estimation relies predominantly on recent interactions with the current or near-current adversary. The adversary update frequency N_{freq} is tuned such that the off-policy agent has sufficient steps to adapt to the current risk distribution before the adversary shifts its strategy. This historical diversity acts as a natural form of domain randomization, preventing the ego from overfitting to specific attack patterns.

Credit assignment in critic-free methods. While critic-based methods (e.g., PPO) rely on a value function $V(s)$ to reduce variance, critic-free methods like GRPO typically utilize sequence-level outcome supervision. In the training of LLMs, it is common to assign the final reward of a completed sequence to all tokens. However, we identify that *directly*

applying this sequence-level supervision to AD tasks leads to severe credit assignment issues, particularly when addressing the long-tail distribution. Our experiments revealed that applying standard outcome supervision leads to training instability and policy collapse after certain steps. This occurs because safety-critical failures (e.g., collisions) often happen at the very end ($t = T$) of a long-horizon episode. Assigning a low return to the entire trajectory incorrectly penalizes the correct driving behaviors exhibited in the early stages of the episode ($t \ll T$), resulting in high-variance gradients that disrupt the fine-tuning phase. On the other hand, implementing standard process supervision (e.g., via Monte Carlo value estimation across rollouts (Guo et al., 2025)) would require the physical simulator to support resetting to arbitrary intermediate states to perform multiple forward rollouts from every timestep. In complex high-fidelity simulators, this requirement introduces substantial engineering complexities regarding state serialization and incurs prohibitive computational overhead.

To resolve this, we propose a *step-aligned group advantage estimator* that provides dense step-level supervision without requiring a learned critic or simulator state resets. Specifically, for each update step, we sample a scenario context X and generate a group of G independent episodes ($G = 6$ in our experiments) starting from the exact same initial state (achieved via scenario seeding) but with different stochastic action realizations. Let $\tau_i = \{(s_t, a_t, r_t)\}_{t=0}^{T_i}$ denote the i -th transition in the group. We implement the following modifications to the advantage estimation:

1. **Calculating returns-to-go:** Instead of the total episode return, we calculate the discounted return-to-go $R_{t,i} = \sum_{k=t}^{T_i} \gamma^{k-t} r_{k,i}$ for each step t in transition i . This ensures that an action is only evaluated based on its consequences.
2. **Step-aligned group normalization:** We compute the advantage $A_{t,i}$ by normalizing $R_{t,i}$ against the returns of other trajectories in the same group at the same time step t , which uses the peer group as a dynamic baseline:

$$A_{t,i} = \frac{R_{t,i} - \mu_t}{\sigma_t + \epsilon}, \quad \text{where } \mu_t = \frac{1}{G} \sum_{j=1}^G R_{t,j}, \quad \sigma_t = \sqrt{\frac{1}{G} \sum_{j=1}^G (R_{t,j} - \mu_t)^2}. \quad (50)$$

3. **Baseline padding:** Since episodes have varying lengths (e.g., due to early termination from crashes), the group size at step t could decrease. To maintain a low-variance baseline, we apply zero-padding to terminated trajectories. If trajectory j ends at $T_j < t$, we set $R_{t,j} = 0$. This ensures the baseline μ_t is always computed over the full group size G , correctly reflecting that survival yields higher future returns than termination.
4. **Advantage clipping:** To prevent single outliers such as rare failures from dominating the gradient and destabilizing the policy, we clip the calculated advantages as: $\hat{A}_{t,i} = \text{clip}(A_{t,i}, -C, C)$, where $C = 5.0$.

Then Eq. 50 is integrated into the standard GRPO loss and optimized via mini-batch gradient descent. This modification provides an efficient and low-variance gradient signal that correctly attributes failure to specific actions leading up to it, without the instability observed in outcome supervision or expensive state resetting.

D.2.4. APPLICATION TO LEARNING-BASED MOTION PLANNING MODELS

In this section, we detail the implementation of applying ADV-0 to fine-tune trajectory planning models. Unlike standard end-to-end RL policies that output control actions directly, motion planners output future trajectories which are then executed by a low-level controller. This introduces challenges regarding re-planning and reward attribution. To address this, we decouple the planning evaluation from environmental execution, inspired by Chen et al. (2025). Note that this framework can be applied to any RL algorithm, and we adopt GRPO as a demonstration.

Model architectures. To demonstrate the versatility of ADV-0, we apply it to two representative categories of state-of-the-art motion planning models:

1. **Autoregressive generation (SMART (Wu et al., 2024)):** SMART formulates motion generation as a next-token prediction task, analogous to LLMs. It discretizes vectorized map data and continuous agent trajectories into sequence tokens, utilizing a decoder-only Transformer to model spatial-temporal dependencies. By autoregressively predicting the next motion token, the model effectively captures complex multi-agent interactions and has demonstrated potential for motion generation and planning.

2. **Multimodal Scoring (PlanTF (Cheng et al., 2024)):** PlanTF is a Transformer-based imitation learning planner designed to address the shortcut learning phenomenon often observed in history-dependent models. It encodes the ego vehicle’s current kinematic states, map polylines, and surrounding agents using a specialized attention-based state dropout encoder to mitigate compounding errors. This architecture allows the planner to generate robust closed-loop trajectories by focusing on the causal factors of the current scene rather than overfitting to historical observations. PlanTF has achieved state-of-the-art in several popular motion planning benchmarks.

Following the standard pretrain-then-finetune practice, we first apply imitation learning to train supervised policies by behavior cloning. To deploy these models in closed-loop simulation, we implement a wrapper policy that executes a re-planning cycle every $N = 10$ simulation steps (1.0s). At each cycle, the planner receives the current observation and generates a trajectory. A PID controller then tracks this trajectory to produce steering and acceleration commands for the underlying physics engine. We employ an advanced PID controller with a dynamic lookahead distance to ensure smooth tracking of the planned path.

Fine-tuning planners via ADV-0 . Directly applying standard RL algorithms to fine-tune trajectory planners is inefficient due to the sparsity of rewards relative to the high-dimensional output space. In addition, the low-level controller executed during a re-planning horizon increases the difficulty of reward credit assignment. To address this, we decouple planning evaluation from execution and implement a state-wise reward model (SWRM) to provide dense supervision directly on the planned trajectories, following Chen et al. (2025). We employ GRPO to fine-tune the planners. The process at each re-planning step t is as follows:

1. **Generation:** The planner generates a group of K candidate trajectories $\{T_1, \dots, T_K\}$ conditioned on the current state s_t . For PlanTF, these are the multimodal outputs; for SMART, we sample K sequences via temperature sampling.
2. **Evaluation:** Instead of rolling out K trajectories in the simulator, we evaluate them immediately using SWRM. SWRM calculates an instant reward r_k for each T_k based on geometric and kinematic properties over a horizon $H = 2.0s$:

$$r(T_k) = w_{\text{prog}} \cdot \Delta_{\text{long}} - w_{\text{coll}} \cdot \mathbb{I}_{\text{coll}} - w_{\text{road}} \cdot \mathbb{I}_{\text{off}} - w_{\text{comf}} \cdot \text{Jerk}, \quad (51)$$

where weights are set to $w_{\text{coll}} = 20.0$, $w_{\text{road}} = 5.0$.

3. **Optimization:** We compute the advantage for each candidate as $A_k = (r_k - \bar{r})/\sigma_r$, where \bar{r} and σ_r are the mean and standard deviation of rewards within the group. The policy is updated to maximize the likelihood of high-advantage trajectories using the GRPO objective:

$$\mathcal{L}_{\text{GRPO}} = -\frac{1}{K} \sum_{k=1}^K \min \left(\frac{\pi_{\theta}(T_k|s_t)}{\pi_{\text{old}}(T_k|s_t)} A_k, \text{clip} \left(\frac{\pi_{\theta}(T_k|s_t)}{\pi_{\text{old}}(T_k|s_t)}, 1 - \epsilon, 1 + \epsilon \right) A_k \right). \quad (52)$$

For PlanTF, we fine-tune the trajectory scoring head and decoder; for SMART, we fine-tune the token prediction logits.

4. **Execution:** The trajectory with the highest SWRM score is selected for execution by the PID controller to advance the environment to the next re-planning step.

For PlanTF, we fine-tune the trajectory scoring head; for SMART, we fine-tune the token prediction head. This approach allows the planner to learn from the adversarial scenarios generated by ADV-0 by explicitly penalizing trajectories that the SWRM identifies as risky, without requiring dense environmental feedback.

Adversarial interaction. The ADV-0 adversary operates in the inner loop as described in the main paper. The adversary generator \mathcal{G}_{ψ} creates challenging scenarios based on the planner’s executed history, and is further updated via IPL. The planner is then fine-tuned via GRPO to propose safer trajectories in response to these generated risks.

D.3. Baselines

We compare ADV-0 against a comprehensive set of baselines, categorized into adversarial scenario generators (methods that create the environment) and closed-loop adversarial training frameworks (methods that train the ego policy).

Backbone model. Consistent with prior works (Zhang et al., 2023; Nie et al., 2025; Stoler et al., 2025), we employ DenseTNT (Gu et al., 2021) as the backbone motion prediction model for the adversarial generator. DenseTNT is an anchor-free, goal-based motion forecasting model capable of generating multimodal distributions of future trajectories, which is known for its high performance on the WOMD benchmark. We initialize the generator using the publicly available pretrained checkpoint, ensuring a fair comparison of the generation capabilities.

Adversarial generators. To evaluate the effectiveness of the generated scenarios, we compare ADV-0 against a comprehensive set of adversarial generation methods, covering optimization-based, learning-based, and sampling-based paradigms:

- **Heuristic (Zhang et al., 2023):** A hand-crafted baseline that modifies the trajectory of the background vehicle to intercept the ego vehicle’s path using Bezier curve fitting. It heuristically generates aggressive cut-ins or emergency braking maneuvers based on the ego vehicle’s position. This serves as an oracle method representing worst-case physical attacks.
- **CAT (Zhang et al., 2023):** A state-of-the-art sampling-based approach that generates adversarial trajectories by resampling from the DenseTNT traffic prior. It selects trajectories that maximize the posterior probability of collision with the ego vehicle’s planned path.
- **KING (Hanselmann et al., 2022):** A gradient-based approach that perturbs adversarial trajectories by backpropagating through a differentiable kinematic bicycle model to minimize the distance to the ego vehicle.
- **AdvTrajOpt (Zhang et al., 2022):** An optimization-based approach that formulates adversarial generation as a trajectory optimization problem. It employs Projected Gradient Descent (PGD) to iteratively modify trajectory waypoints to induce collisions.
- **SEAL (Stoler et al., 2025):** A skill-enabled adversary that combines a learned objective function with a reactive policy. It utilizes a scoring network to predict collision criticality and ego behavior deviation.
- **GOOSE (Ransiek et al., 2024):** A goal-conditioned RL framework. The adversary is modeled as an RL agent that learns to manipulate the control points of Non-Uniform Rational B-Splines (NURBS) to construct safety-critical trajectories.
- **SAGE (Nie et al., 2025):** A recent preference alignment framework that fine-tunes motion generation models using pairs of trajectories. It learns to balance adversariality and realism, allowing for test-time steerability via weight interpolation between adversarial and realistic expert models.

Adversarial training frameworks. To demonstrate the effectiveness of our closed-loop training pipeline, we compare ADV-0 with the following training paradigms. All methods use the same outer-loop ego policy training structure but differ in how the training environment is generated and how the inner and outer loops are integrated:

- **Replay (w/o Adversary):** The ego agent is trained purely on the original log-replay scenarios from WOMD without any adversarial modification. This serves as a lower bound for performance.
- **Heuristic training:** The ego agent is trained against the Heuristic rule-based generator described above.
- **CAT:** The state-of-the-art closed-loop training framework where the ego agent is trained against the CAT generator. The generator selects adversarial trajectories based on collision probability against the latest ego policy but does not update its policy via preference learning during the training loop.
- **ADV-0 w/o IPL:** An ablation variant of ADV-0 where IPL is removed and the adversary is not fine-tuned. It relies solely on energy-based sampling from the pretrained backbone. This isolates the contribution of the evolving adversary.

For fair comparison, all adversarial training methods (CAT, ADV-0, etc.) utilize the same curriculum learning schedule regarding the frequency and intensity of adversarial encounters. Note that we explicitly exclude comparisons with standard adversarial RL frameworks, such as RARL (Pinto et al., 2017; Ma et al., 2018) or observation-based perturbation methods (Tessler et al., 2019; Zhang et al., 2020a) due to two key factors: (1) They primarily focus on perturbations to observations or state vectors. In contrast, ADV-0 targets behavioral robustness by altering the transition dynamics via trajectory generation.

(2) Standard adversarial RL models the adversary as an agent with a low-dimensional action space. Our setting involves noisy real-world traffic data and the adversary outputs high-dimensional continuous trajectories. Training a standard RL adversary from scratch to generate effective trajectories in this noisy environment is computationally intractable and fails to converge in our preliminary experiments.

D.4. Hyperparameters

We provide the detailed hyperparameters used in our experiments to facilitate reproducibility. Table 16 lists the parameters for the various RL algorithms used to train the ego agent. Table 20 details the hyperparameters for the ADV-0 framework, including the IPL fine-tuning process and the min-max training schedule.

Table 16. Hyperparameters for different RL algorithms used in the experiments.

Table 17. TD3		Table 18. SAC & SAC-Lag		Table 19. PPO, PPO-Lag & GRPO	
Hyper-parameter	Value	Hyper-parameter	Value	Hyper-parameter	Value
Discount Factor γ	0.99	Discount Factor γ	0.99	Discount Factor γ	0.99
Batch Size	256	Batch Size	256	Batch Size	256
Actor Learning Rate	3e-4	Learning Rate	3e-4	Learning Rate	3e-5
Critic Learning Rate	3e-4	Target Update τ	0.005	Update Timestep	4096
Target Update τ	0.005	Entropy α	0.2 (Auto)	Epochs per Update	10
Policy Delay	2	Cost Coefficient	0.5	Clip Ratio	0.2
Exploration Noise	0.1	<i>SAC-Lag Specific</i>		GAE Lambda λ	0.95
Policy Noise	0.2	Cost Limit	0.3	Entropy Coefficient	0.01
Noise Clip	0.5	Lagrangian LR	5e-2	Value Coefficient	0.5
				<i>Algorithm Specific</i>	
				Cost Limit (PPO-Lag)	0.4
				Lagrangian LR (Lag)	5e-2
				Group Size (GRPO)	6
				KL Beta (GRPO)	0.001

Table 20. Hyperparameters for ADV-0 Framework and IPL Fine-tuning.

Module	Parameter	Value
Backbone (DenseTNT)	Hidden Size	128
	Sub-graph Depth	3
	Global-graph Depth	1
	Trajectory Modes (K)	32
	NMS Threshold	7.2
IPL Fine-tuning	Learning Rate	5e-6
	Temperature (τ)	0.05
	Optimizer	AdamW
	Scheduler	CosineAnnealing
	Gradient Accumulation Steps	16
	Pairs per Scenario	8
	Reward Margin	5.0
Spatial Diversity Threshold	2.0 m	
Min-Max Schedule (RARL)	Adversary Update Frequency	Every 5 Ego Updates
	Adversary Training Iterations	5 Epochs per Block
	Adversary Training Batch Size	32 Scenarios
	Adversarial Sampling Temperature	0.1
	Max Training Timesteps	1×10^6
	Opponent Trajectory Candidates	32
	Ego History Buffer Length	5
Min Probability (Curriculum)	0.1	